Fermi National Accelerator Laboratory

FERMILAB-Pub-94/010-A
January 1994

COSMIC RAY MODELS FOR EARLY GALACTIC LITHIUM, BERYLLIUM, AND BORON PRODUCTION†

Brian D. Fields[1], Keith A. Olive[2], and David N. Schramm[1,3]

[1] *The University of Chicago, Chicago, IL 60637-1433*
[2] *School of Physics and Astronomy, University of Minnesota, Minneapolis, MN 55455*
[3] *NASA/Fermilab Astrophysics Center, Fermi National Accelerator Laboratory, Batavia, IL 60510-0500*

ABSTRACT

To better understand the early galactic production of Li, Be, and B by cosmic ray spallation and fusion reactions, the dependence of these production rates on cosmic ray models and model parameters is examined. The sensitivity of elemental and isotopic production to the cosmic ray pathlength magnitude and energy dependence, source spectrum, spallation kinematics, and cross section uncertainties is studied. Changes in these model features, particularly those features related to confinement, are shown to alter the Be- and B-versus-Fe slopes from a naïve quadratic relation. The implications of our results for the diffuse γ-ray background are examined, and the role of chemical evolution and its relation to our results is noted. It is also noted that the unmeasured high energy behavior of $\alpha + \alpha$ fusion can lead to effects as large as a factor of 2 in the resultant yields. Future data should enable Population II Li, Be, and B abundances to constrain cosmic ray models for the early Galaxy.

---

†submitted to *The Astrophysical Journal*

1 Introduction

The Population I abundances of ^{6}Li, Be, and B (LiBeB) have been thought for some time to have their origin in spallation and fusion processes between cosmic ray and interstellar medium (ISM) nuclei (see, e.g., Reeves, Folwer, & Hoyle 1970; Meneguzzi, Audouze, & Reeves 1971; Walker, Mathews, & Viola 1985). In the past few years these elements have been sought extreme Population II dwarfs, stars well known to exhibit the "Spite plateau" in lithium (Spite & Spite 1982), which is understood to indicate the primordial ^{7}Li abundance (Walker, Steigman, Schramm, Olive, & Kang 1991). Recently these same Pop II stars have also been shown to additionally contain Be, (Rebolo et al. 1988a; Ryan et al. 1990, 1992; Gilmore et al. 1992a, 1992b; Boesgaard & King 1993) B, (Duncan, Lambert, & Lemke 1992) and most recently ^{6}Li (Smith, Lambert, & Nissen 1992). These abundances provide important clues about the early galaxy, and cosmic rays have been considered the most likely production mechanism for LiBeB in these stars as well (Steigman & Walker 1992 (SW); Prantzos, Cassé, & Vangioni-Flam 1992 (PCV); Walker et al. 1993 (WSSOF); Steigman et al. 1993 (SFOSW)).

If indeed the extreme population II LiBeB arise from cosmic ray interactions, the study of their isotopic abundances opens an important window on astrophysics. In principle, we may be able to gain insight on early cosmic rays, as well as early star formation rates and chemical evolution (e.g. PCV; Fields, Schramm, & Truran 1993; Silk & Schramm 1992). In addition, associated with these early cosmic ray events is an appreciable gamma-ray flux which would contribute (perhaps significantly) to the present diffuse gamma-ray background (Silk & Schramm 1992; Prantzos & Cassé 1993). The early cosmic ray scenario is also of importance to cosmology. One may use the results of a galactic cosmic-ray (GCR) spallation and fusion model to help infer primordial ^{7}Li from the observed Li abundance (Olive & Schramm 1993). One may also use the GCR model's cosmic ray spallation information on the Li isotopes, compared with their observed abundances, to deduce the amount of possible stellar depletion (SFOSW).

Our previous work (WS, WSSOF, SFOSW) was an attempt at a relatively model-independent approach. Without assuming a specific model (of cosmic ray or galactic chemical evolution) we concentrated on testing the consistency of standard GCR models with the recent LiBeB observations and with primordial nucleosynthesis where possible by examining elemental and isotopic abundance ratios. In another approach, Gilmore et al. (1992b), Feltzing & Gustaffson (1993), Prantzos (1993), Prantzos & Cassé (1993), Pagel (1993), and particularly PCV have chosen to adopt a particular detailed model of early galactic chemical and cosmic ray evolution to examine its predictions and compare with observations.

In this paper we will examine in detail the dependence of the LiBeB abundances produced by GCR nucleosynthesis on the uncertainties of, or allowed variations in, the cosmic-ray model. As such, we will discuss the uncertainties in cosmic ray models. After a brief review of the data, we present some model options in section 3. Our assumptions

regarding the evolution of the abundances of α, C, N, and O are discussed in section 4. We address the issue of the Be and B slopes versus [Fe/H] in section 5. The cosmic-ray spectrum and the confinement of cosmic rays will be discussed in section 6. We also explore implications of these models on γ-ray production in section 7. We draw conclusions in section 8.

2 LiBeB Abundance Data

To make this work as self-contained as possible, we show in table I LiBeB isotopic abundances observed in Pop II halo dwarf stars. We list those stars in which at least two light elements have been observed as we will for the most part be primarily interested in elemental or, even better, isotopic ratios. The notation we employ below and use throughout the paper is that [X/H] represents the log abundance relative to the solar abundance, namely $\log(X/H) - \log(X/H)_\odot$ and $[X] = 12 + \log(X/H)$. In the table, the iron abundance represents an unweighted "world" average. For the other abundances, a weighted average is given. The ^{6}Li abundance was taken from Smith et al. (1993). The ^{7}Li abundances were taken from Spite & Spite (1982,1986); Spite et al. (1984); Hobbs and Duncan (1987); Rebolo et al. (1988b); Hobbs & Thorburn (1991); and Pilachowski et al. (1993). The ^{9}Be abundances were taken from Rebolo et al. (1988a); Ryan et al. (1992); Gilmore et al. (1992a,b); Molaro, Castelli, & Pasquini (1993); and Boesgaard & King (1993). Finally, the boron abundances were taken from Duncan et al. (1992).

The ratios of ^{6}Li to ^{7}Li, Li to Be and of B to Be are the observed ratios. Because, for Pop II, the dominant contribution to the ^{7}Li abundance comes from primordial nucleosynthesis rather than GCR nucleosynthesis, a certain degree of caution is necessary when comparing the first two of these ratios to the predictions we discuss below. On the other hand because there is no appreciable big bang source for either Be or B (Thomas et al., 1993), the ratio of these two may be compared (unless there is an additional primary source for ^{11}B as discussed in Dearborn et al. (1988), Woosley et al. (1990), and Olive et al. (1993)).

Because of the importance of the B/Be ratio, we note that the values given in the table for Be and the ratio B/Be, are averages over observations by several groups. These observations themselves show some spread which may be significant. For the star HD19445, beryllium upper limits were obtained by Rebolo et al. (1988a), giving $[Be] < 0.3$, and $B/Be > 1.3$, Ryan et al. (1990) found the upper limit $[Be] < -0.3$ and hence $B/Be > 5$ which should be compared with the value of 3.5 in the table which represents the only positive identification of Be in this star by Boesgaard and King (1993) and is slightly discrepant with the upper limit of Ryan et al. For HD140283, we have measurements of Be by three groups: $[Be] = -1.25 \pm 0.4$ from Ryan et al. (1992) giving $B/Be = 14 \pm 14$; $[Be] = -0.97 \pm 0.25$ from Gilmore et al. (1992) giving $B/Be = 7 \pm 5$; $[Be] < -0.90$ from Molaro, Castelli, & Pasquini (1993), giving $B/Be > 6$; and

[Be] = -0.78 ± 0.14 from Boesgaard and King (1993) giving B/Be = 5 ± 3. Finally for HD201891, [Be] = 0.4 ± 0.4 from Rebolo et al. (1988a) giving B/Be = 20 ± 26 and [Be] = 0.67 ± 0.1 from Boesgaard and King (1993) giving B/Be = 11 ± 10. As one can see there appears to be a wide range in values (and uncertainties) in this ratio, and the values given my be completely dominated by systematics which are poorly accounted for in the stated error. In particular, ratios are most useful if constant surface temperature and surface gravity assumptions are used in the specific elemental determinations. Unfortunately, this is not yet the case.

Indeed it is the uncertainties in these measurements and in the averages of these measurements which are themselves uncertain. Namely, the *treatment* of systematic errors is far from systematic. The conversion of line strengthes to abundances involves inferences on the surface temperature and surface gravity of the star. Most observational determinations have been made using differents sets of inputs. Though one can ascribe some uncertainty to chosen values of these inputs, it is not always clear to what extent these systematic errors have been incorporated into the quoted so-called statistical error, and different authors make divergent assumptions on the uncertainty of their assumed stellar parameters. Furthermore any average will surely underestimate the true error because of the mistreatment of systematic errors. Thus it is our feeling that B/Be and Li/Be ratios are extremely uncertain.

TABLE 1. OBSERVED POP II ABUNDANCES OF LIBEB ISOTOPES

STAR	[Fe/H]	Li	[Be]	[B]	$^6Li/^7Li$	Li/Be*	B/Be*
HD16031	-1.9	2.03 ± 0.2	-0.37 ± 0.25			251 ± 185	
HD19445	-2.1	2.07 ± 0.07	-0.14 ± 0.1	0.4 ± 0.2		162 ± 46	3.5 ± 1.8
HD84937	-2.2	2.11 ± 0.07	-0.85 ± 0.19		0.05 ± 0.02	912 ± 425	
HD94028	-1.6	2.10 ± 0.08	0.44 ± 0.1			46 ± 13	
HD132475	-1.6	2.05 ± 0.09	0.60 ± 0.3			28 ± 20	
HD134169	-1.2	2.20 ± 0.08	0.71 ± 0.11			31 ± 10	
HD140283	-2.6	2.08 ± 0.06	-0.87 ± 0.11	-0.1 ± 0.2		891 ± 262	6 ± 3
HD160617	-1.9	2.22 ± 0.12	-0.47 ± 0.18			490 ± 244	
HD189558	-1.3	2.01 ± 0.12	0.89 ± 0.33			13 ± 11	
HD194598	-1.4	2.00 ± 0.2	0.37 ± 0.12			43 ± 23	
HD201891	-1.3	1.97 ± 0.07	0.65 ± 0.1	1.7 ± 0.4		21 ± 6	11 ± 11
BD23°3912	-1.5	2.37 ± 0.08	0.30 ± 0.4			117 ± 110	

*Ratios are extremely uncertain due to inadequate treatment of systematics.
Formal errors on ratios are underestimates.

3 Cosmic Ray Models for LiBeB Spallation Production

Currently studied models for LiBeB production are based on the work of Reeves, Fowler, and Hoyle (1970) and the more detailed follow-up work of Meneguzzi, Audouze, and Reeves (1971). They describe cosmic ray propagation via the simple leaky box model. This assumes a spatially homogeneous distribution of sources, cosmic rays, and interstellar material. Within this model, the propagation equation is

$$\frac{\partial N_A}{\partial t} = J_A + \frac{\partial (b_A N_A)}{\partial T} - \frac{1}{\tau_{eff}} N_A \tag{1}$$

Here $N_A = N_A(t,T)$, is the number density of cosmic ray isotopes $A = LiBeB$ at time t with energy (per nucleon) between T and $T + dT$. Note that eq. (1) is the general propagation expression for A a primary or secondary species, with different terms being important for each. The first term on the righthand side, J_A, includes all sources for A:

$$J_A(T) = Q_A(T) + \sum_{ij} n_j \int_{T_{th}^{nuc}}^{\infty} dT' \phi_i(T') \frac{d\sigma_{ij}^A}{dT}(T,T') \ . \tag{2}$$

Here $Q_A(T)$ is a possible galactic source of A, given as a number rate per volume and per unit energy; and spallation production of A appears in the sum runs over projectiles i and targets j. Additionally, $\phi_i = N_i v_i$ is the cosmic ray flux spectrum of species i and, σ_{ij}^A is the cross section for the process $i + j \rightarrow A + \cdots$. The second term of propagation equation (1) energy losses to the ISM, with $b_A = -(\partial T/\partial t)_A$ allows for ionization from the Galaxy. The third term of the propagation equation accounts for catastrophic cosmic ray losses,

$$\frac{1}{\tau_{eff}} = \sum_i \sigma_{iA}^{inel} v_A n_i + \frac{1}{\tau_{esc}} \tag{3}$$

with σ_{iA}^{inel} encoding spallation losses of A in the ISM, and $\tau_{esc}(T)$ being the lifetime for cosmic rays against escape.

The propagation equation (1) is solved for the case of a steady state, $\partial N/\partial t = 0$, in which cosmic ray production is in equilibrium with the losses. One thus obtains the *spectrum* N of these elements, propagated from their source J. At present, we will ignore losses due to inelastic nuclear collisions, valid when $\tau_{esc}^{-1} \gg n_i \sigma_{iA}^{inel} v_A$ (but see section 6.1). We assume that the primary cosmic ray species p, α, and CNO, have some homogeneous galactic source $J = Q$, and negligible spallation production or losses: $\sigma = 0$. Writing the solution for these in terms of the cosmic ray flux $\phi = Nv$, we have

$$\phi_i(T) = \frac{1}{w_i(T)} \int_T^{\infty} dT' q_i(T') \exp\left(-\left[R_i(T') - R_i(T)\right]/\Lambda\right) \tag{4}$$

where $w_i = b_i/\rho_{ISM}v$, and $q_i = Q_i/\rho_{ISM}$, and $i = p$, α, CNO. Also, $R_A(T_A) = \int_0^{T_A} dT'/(\partial T'/\partial X)_{ISM}$ is the ionization range which characterizes the average amount of material a particle with energy T_A can travel before ionization losses will stop it (expressed in $\mathrm{g\,cm^{-2}}$, as $X = \rho_{ISM}vt$). The ionization ranges were taken from Northcliffe and Schilling (1970) for low LiBeB energies (< 12 MeV/nucleon) at which partial charge screening effects are important, and from Janni (1982) for higher energies, using the scaling law

$$R_A(Z;T) = A/Z^2\, R_p(T)\,. \tag{5}$$

Here T the kinetic energy per nucleon and R_p is the proton range.

In figure 1 we plot the proton and α fluxes ϕ_i calculated from eq. (4). To show the effect of energy losses on the propagated flux, we also plot Λq_i, the solution of eq. (1) for negligible energy losses ($b_i \approx 0$). As we will discuss below in sections 5 and 6.1, these losses are important at low energies and negligible at high ones. This is manifest in figure 1, which shows the scaling $\phi = \Lambda q$ to be followed closely at high energies, while at low energies the ionization energy losses significantly reduce the propagated flux from this scaling. This behavior is qualitatively similar for the two source types we consider; propagation differences at low energies are discussed in section 6.1.

In solving the propagation equation for the secondary elements LiBeB, the source term J is assumed to have no primary source component, i.e. $Q = 0$. The exclusive production of these elements occurs via spallation between the primaries and the ISM: $\sigma_{ij}^A \neq 0$. One can write an expression like eq. (4) for LiBeB, giving their cosmic ray spectrum. What we wish to know, however, is not this steady-state spectrum but instead the amount of LiBeB thermalized and added to the ISM. To compute this from the LiBeB spectrum one assumes that all such nuclei below some threshold kinetic energy T_{therm} are thermalized and then one examines the LiBeB current $b_A N_A(T_{therm})$ below this threshold. Below the lowest spallation threshold there is no source term in eq. (1) for LiBeB, and the ionization loss term is much larger than the escape term. Thus to a good approximation the propagation equation (1) reads

$$\frac{\partial}{\partial T} b_A N_A(T) = 0\ , T \leq T_{th}^{nuc} \tag{6}$$

and so the LiBeB current $b_A N_A(T_{therm})$ is constant for T_{therm} below spallation production thresholds. One may thus choose any $T_{therm} \leq T_{th}^{nuc}$ at which to evaluate this current; we choose ours to be right at threshold.

With this method of computing the production rate of LiBeB via evaluation of the subthreshold LiBeB current, we can write the rate of LiBeB accumulation in the ISM as

$$\frac{dy_A(t)}{dt} = \sum_{ij} y_j(t) \int_{T_{th}^{nuc}}^{\infty} dT\ \phi_i(T,t)\ \sigma_{ij}^A(T)\ S_A\left[T_A(T), t\right] \tag{7}$$

where $A = {}^{6,7}\mathrm{Li}$, ${}^9\mathrm{Be}$, ${}^{10}\mathrm{B}$, $y_A = n_A/n_H$, the ϕ_i come from eq. (4), and we have ignored the small time variation of n_H.

The factor $S_A(T_A, t)$ accounts for the energy loss of nucleus A in the ISM and gives the probability of its capture and thermalization; it is a function of the lab energy T_A of the daughter nucleus A, as well as the epoch t, and is given by

$$S_A(T_A, t) = \exp\left[-\left\{R_A(T_A) - R_A(T_{therm})\right\}/\Lambda(t)\right] \tag{8}$$

These energy losses in the ISM serve to trap the spallation products and so to allow them to contribute to the LiBeB finally thermalized in the ISM. This process competes with the the spallation products' escape from the galaxy, quantified by the escape rate τ_{esc}^{-1} of eq. (1). This quantity appears in eq. (8) through $\Lambda = \rho_{ISM} v \tau_{esc}$ the (possibly) energy-dependent average pathlength[1], also in g cm^{-2}. Note that as τ_{esc} sets the scale for the cosmic ray residence time before escape, Λ is the amount of matter traversed before escape. As any $T_{therm} \leq T_{th}^{nuc}$ gives $R(T_{therm}) \ll \Lambda$, we may put $S_A \simeq \exp(-R_A/\Lambda)$. For "forward" kinematics, with a light cosmic ray nucleus impinging on a stationary, heavy ISM nucleus, T_A is small for typical spallation energies, and so $R_A \ll \Lambda$ and $S_A \simeq 1$. For "inverse" kinematics, with a heavy cosmic ray nucleus on a light ISM particle, S_A can differ significantly from unity and the LiBeB yields are reduced accordingly.

Following Walker et al. (1992), we put

$$q_i(T, t) = y_i^{CR}(t)\, q_p(T, t) \tag{9}$$

with i = p,α, CNO: i.e., we posit the constancy of the cosmic ray isotopic and elemental ratios at the source and over the entire energy spectrum. We then choose to make the more serious assumption that we may express the proton source strength in the separable form

$$q_p(T, t) = q_p(T)\, f(t). \tag{10}$$

We will in fact consider various Population II source spectra q (see section 6.2), but we will not allow a fully general energy or time dependence. While this has the immediate advantage of simplifying the calculations, one may view this assumption as a postulation that the present mechanism of cosmic ray acceleration does not differ dramatically over time in its energetics, but only in its net cosmic ray output.

In our analysis of cosmic ray model features, and in the accompanying figures, we will concern ourselves with the effect on the LiBeB production rates—or rather their ratios—as calculated by eq. (7). Given a set of cosmic ray and ISM abundances, and a confinement parameter Λ, these rates may be evaluated numerically. As in previous work, we used empirical values of partial cross sections tabulated in by Read and Viola (1984). To proceed further and integrate the rates to get the LiBeB yields would require a full model for cosmic ray and chemical evolution. We discuss this issue in the next section.

[1]By writing the argument of the exponential in S_A as we have in eq. (8), we are assuming Λ to be constant in energy. For further discussion see section 6.1.

As a cosmic ray model of propagation, the above amounts to the simple leaky box (reviewed by, e.g., Ceasarsky 1980, 1987). This is the simplest model used to describe cosmic rays today, and as such has obvious computational advantages. While the simplicity of the leaky box makes it a useful tool, it is physically unrealistic and thus, in some cases, quite inaccurate. A proper treatment of cosmic ray propagation must explicitly include diffusion effects only sketched with the leaky box confinement parameter Λ. Also, a proper model must abandon the simple leaky box assumption of spatial homogeneity of sources and interstellar material. Despite these shortcomings, however, we will follow previous authors and adopt this model in what follows, both for the above pragmatic reasons and moreover because the epoch we consider is so poorly understood in its relevant details that adoption of a more detailed description is not warranted at the present time.

4 The Role of Chemical Evolution

Although we can calculate the rates in eq. (7), for a given set of parameters, using well-understood physics, to integrate these rates requires knowledge of the chemical and dynamical evolution of the cosmic ray and ISM species in the Galaxy's early history. Such knowledge is sketchy at present, but some reasonable assumptions will prove fruitful.

If we assume that the H and He abundances do not change much from their values as set by the big bang, we have

$$\begin{aligned} H(t) &\approx H^{BB} \\ y_{He}(t) &\approx y_{He}^{BB} \approx 0.08\,. \end{aligned} \tag{11}$$

If we further assume that the CNO nuclides evolve at the same rate, so that their ratios remain constant within the early epoch considered here, we put

$$\frac{y_C(t)}{y_C^{OBS}} = \frac{y_N(t)}{y_N^{OBS}} = \frac{y_O(t)}{y_O^{OBS}}\,. \tag{12}$$

assumed to hold for times t less than the galactic age τ at the birth of the Be or B star having CNO abundances denoted here as OBS. One should interpret equation 12 with some care, as approximation of constant C:N:O ratios is not strictly true. We expect these elements to have different sources: O is made in type II supernovae but C and N are made primarily in intermediate mass stars. Thus any differences in the evolution of these sites will result in differences in the abundance ratios. Fortunately, large differences between CN and O production are only important at early times, and the observed Pop II CNO abundances are consistent with constant C:N:O over the timescales important here. One should note, however, that the O/CNFe ratio, though the roughly constant,

does exceed the solar ratio. This comes about because of the predominance at this epoch of type II supernovae over type I's. The effect is important for our purposes, as spallation off of O gives a lower B/Be ratio than spallation off of C.

We again simplify by extrapolating the present relation between abundances of cosmic ray and ISM species, namely we assume that the relative enhancement of the cosmic ray CNO abundances over interstellar CNO abundances has remain constant in time. We put

$$\frac{y_i^{CR}(t)}{y_i(t)} = \left(\frac{y_i^{CR}}{y_i}\right)_{present} \tag{13}$$

where $i = CNO$ and the righthand side denotes the present value. We will in fact adopt the stronger assumption, made in most work, that

$$y^{CR}(t) = y^{ISM}(t) \tag{14}$$

but we note that this assertion is false for the present cosmic rays. In particular, Asakimori et al (1993), and references therein, report that found a H/O depletion of about a factor of 2 relative to solar. The proton-to-helium ratio in the cosmic rays is energy dependent and varies from ~ 0.2 at the lowest measured energies to ~ 0.05 at the highest energies which interest us here. Additionally, as shown in Buckeley et al (1993), He/O in the cosmic rays is depleted by a factor of ~ 4.6 relative to its local galactic value. In this paper we have normalized to the protons, and thus adopting the observational results would amount to reducing $y_{\rm He}$ by 2.3, and enhancing $y_{\rm CNO}$ by a factor of 2. We will instead use eq. (14) to allow comparison of ours with previous results. Bear in mind, however, that the cosmic ray abundance scalings are uncertain by at least a factor of 2.

One proposed model which clearly contradicts this assumption is that which explains the Be/O constancy by having the CNO either as targets or projectiles be at supernova production abundances. We may model this behavior by putting

$$y_O^{CR}(t) = y_O^{supernova} \simeq y_O^{present} \gg y_O^{OBS} \tag{15}$$

In what follows, however, wherever not explicitly noted otherwise, eq. (13) will be assumed to hold.

If we allow the confinement pathlength to vary with time, then as we will see below, we may not further simplify the rate equation (7), or the integral that is its solution. If the confinement is taken to be constant in time—a dubious proposition, as we shall see—we may now separate the *propagated* flux:

$$\phi(T,t) = f(t)\varphi(T)\,. \tag{16}$$

This allows one to write the solution to the rate equation as a sum of terms, each of which has a factor that involves an integral over time and a factor involving an integral over energy:

$$y_A(\tau) = \sum_{ij} \Delta_{ij} \langle \Phi \sigma_{ij}^A \rangle \tag{17}$$

with the "exposure time" given by

$$\Delta_{ij}(\tau) = \int_0^\tau dt\, y_j(t)\, y_i^{CR}(t)\, f(t) \tag{18}$$

with τ is the age of the Galaxy at the birth of the star in question, and the "reduced rate" is

$$\langle \Phi \sigma_{ij}^A \rangle = \int_{T_{th}^{nuc}}^\infty dT\, \phi_i(T,t)\, \sigma_{ij}^A(T)\, S_A(T_A,t)\ . \tag{19}$$

Note that these factors are different for forward and inverse kinematics, that is, $\langle \Phi \sigma_{ij}^A \rangle_f \neq \langle \Phi \sigma_{ij}^A \rangle_r$. As mentioned above, this stems from the longer range and greater chance of escape for the fast A–nuclei produced in inverse kinematic collisions.

With the assumptions made thus far in this section—most importantly, that of the time constancy of Λ, the number of independent exposure times may be reduced to three (SW, WSSOF):

$$\Delta_{ij} = \begin{cases} \Delta_{\alpha,\alpha} & i = j = \alpha \\ \Delta_{p,O}^{ISM} & \text{forward kinematics} \\ \Delta_{p,O}^{CR} & \text{inverse kinematics} \end{cases} \tag{20}$$

Of these, we will take $\Delta_{\alpha,\alpha}$ as the fiducial quantity, as it measures the integrated flux enhancement exclusively (ie with no explicit dependence on chemical evolution)

$$\Delta_{\alpha,\alpha} = \int_0^\tau dt\, f(t) \tag{21}$$

We then define the quantity $\langle O/H \rangle$, which is a measure of the average abundance of oxygen relative to hydrogen,:

$$\begin{aligned} \langle O/H \rangle_{ISM} &\equiv \frac{\Delta_{p,O}^{ISM}}{\Delta_{\alpha,\alpha}} \\ &= \frac{\int_0^\tau dt\, y_O^{ISM}(t) f(t)}{\int_0^\tau dt\, f(t)} \end{aligned} \tag{22}$$

with a similar expression for $\langle O/H \rangle_{CR}$. Note that $\langle O/H \rangle$ is to the weighted average of O/H at time τ. This average weighted by the net flux enhancement $f(t)$, and is normalized.

With this notation we have

$$y_{Be,B} = \Delta_{\alpha\alpha} \left(\langle O/H \rangle_{ISM} \sum_{ij}{}' \langle \Phi \sigma_{ij}^{Be,B} \rangle_f + \langle O/H \rangle_{CR} \sum_{ij}{}' \langle \Phi \sigma_{ij}^{Be,B} \rangle_r \right) \tag{23}$$

$$y_{Li} = \Delta_{\alpha\alpha} \left[\langle \Phi \sigma_{\alpha\alpha}^{Li} \rangle + \left(\langle O/H \rangle_{ISM} \sum_{ij}{}' \langle \Phi \sigma_{ij}^{Li} \rangle_f + \langle O/H \rangle_{CR} \sum_{ij}{}' \langle \Phi \sigma_{ij}^{Li} \rangle_r \right) \right] \tag{24}$$

where the prime on the summation indicates that any $i = j = \alpha$ term has been deleted. Note that the ratio of LiBeB production rates, i.e. of eqs. (23) and (24), does not depend explicitly on $\Delta_{\alpha\alpha}$. However, the flux enhancement appears via the strong dependence on $\langle O/H \rangle$, which includes a factor of $\Delta_{\alpha\alpha}$ in its definition.

From eq. (17) it is clear that chemical evolution effects are encoded into the LiBeB abundances in terms of exposure time, in which these effects are convolved with cosmic ray flux evolution. While this means that the absolute abundances are dependent on chemical evolution, it also means that the relative abundances are much less so if the LiBeB isotopes compared originate in similar processes. This is the case with Be and B, which are both produced in pure spallation events, as opposed to Li, which is produced not only by spallation but also in $\alpha+\alpha$ fusion events. This point was stressed by WSSOF, who noted that the ratio B/Be is the *least* dependent on our knowledge of the early galaxy and of early cosmic rays. WSSOF showed that any model for early cosmic ray LiBeB production yields a B/Be ratio lying within the range $7.5 \leq \mathrm{B/Be} \leq 17$. One might compare this with the average of the observed values in the most extreme Population II dwarf, HD 140283, which has $\mathrm{B/Be} = 6 \pm 3$. This ratio is the strongest prediction of the cosmic ray model. However, while the theoretical prediction is firm, particularly in setting a lower bound to the B/Be ratio from cosmic rays, the experimental ratio is still difficult to obtain reliably. As discussed in section 2, the true errors to the measured value, when including systematic uncertainties, are certainly larger than the simple weighted mean we quote here. Comparisons with the observations are thus not all that compelling at the present time.

Under the assumption that there is no additional (primary) source for ^{11}B, the B/Be ratio is weakly dependent on chemical and cosmic ray evolution. However, it is well known that the predicted value of the ^{10}B to ^{11}B ratio by GCR nucleosynthesis yields a ratio of about two, whereas the observed ratio in meteorites is just over four. Dearborn et al. (1988) proposed a possible thermonuclear production of ^{11}B in Type II supernovae, and Woosley et al. (1992) had suggested that neutrino processes during supernovae may yield a significant abundance of ^{11}B. Both suggestions are tested in a GCR and chemical evolution model by Olive et al. (1993), where it was found that while the ^{11}B-^{10}B ratio, could be brought into agreement with the observation, the supernova sources, added in a significant primary source for ^{11}B which upsets the constancy of the B to Be ratio as a function of metallicity. Though the data seem to disfavor this primary source which predicts a B/Be ratio in excess of 50 at $[\mathrm{Fe/H}] < -3$, the scant amount of data at present can not conclusively eliminate this possibility.

In contrast, the ratios of Li with Be and B are always strongly dependent upon chemical and cosmic ray evolution because of the $\alpha - \alpha$ production channel for Li. In addition, the dominant component of the observed ^{7}Li is primordial, further complicating comparison of Pop II LiBeB with GCR nucleosynthesis predictions.

5 The Be and B *versus* Fe Relations

Many have suggested that since Be and B arise from the interaction of stellar nucleosynthesis products with cosmic rays, they should vary quadratically with elements, e.g. O, which form their targets. This dependence is argued to follow from the fact that cosmic ray sources are presumed to be supernovae which are the producers of the oxygen targets. Of course such an assumption is extremely naïve since cosmic rays have a large confinement time and hence the instantaneous recycling approximation that yields this quadratic dependence is quite inappropriate. Even more significant is the fact that the data does not show this dependence and is instead best fit by a Be slope relative to O that is much closer to 1 than to 2. This discrepancy has received some attention and has even been mis-interpreted it as a failure of the cosmic ray model. It is obvious that reports of the death of early cosmic ray LiBeB are, however, greatly exaggerated.

Let us now go through the logic in greater detail. The argument for a quadratic scaling of Be and B with O proceeds from these assumptions: (*a*) Type II supernovae are the dominant source for O, so one expects a relation to N_{SN}, the total integrated number of supernovae, of the form $O \propto N_{SN}$. (*b*) Supernovae are also likely to be the acceleration site for cosmic rays, so one might naïvely expect nthe cosmic ray flux ϕ to vary with the current *rate* at which these acceleration sites are created: $\phi \propto dN_{SN}/dt$ if we ignore confinement and assume instantaneous recycling of the cosmic rays. Put slightly differently, in the leaky box model we have adopted, we have assumed an equilibrium to hold between the rate at which cosmic rays are lost and the rate at which they are created. Thus in this model one can argue that the cosmic ray flux is indeed proportional to this creation rate. Then, taking the essential pieces of the rate equation (7), we obtain the naïve result

$$\begin{aligned} d\mathrm{Be}/dt &\propto \mathrm{O}\phi \\ &\propto N_{SN} dN_{SN}/dt \\ \Longrightarrow \mathrm{Be} &\propto \mathrm{O}^2 \end{aligned} \tag{25}$$

which gives the advertised quadratic dependence, with an analogous equation for B evolution.

While assumption (*a*) seems solid, assumption (*b*) is not because it accounts for evolution of cosmic ray sources but not for changes in confinement. Indeed the evolution of Λ is the critical feature allowing one to avoid the naïve secondary-to-primary ratio for the B- or Be-to-O ratio of eq. 25. For a given source density q of *primary* cosmic ray elements (at some instant t), the propagated flux ϕ increases with Λ, as at larger Λ the cosmic rays traverse more matter before escape and so the steady state between production and escape is reached at a higher flux. In the limit of no energy losses, valid at high energy, the relation is $\phi = \Lambda q$. With energy losses, this relation is energy dependent, but for the total flux PCV find that it varies roughly as $\phi \propto \Lambda^{1/2}$. Thus we

should alter the cosmic ray flux scaling to be $\phi(t) \propto \Lambda^{1/2}(t) N_{SN}(t)$, and it follows that changes in the early confinement alters the cosmic ray flux, and its associated LiBeB production. Specifically, in the place of eq. 25, we have the more general relation

$$\begin{aligned} d\mathrm{Be}/dt &\propto \Lambda^n \mathrm{O} d\mathrm{O}/dt \\ \Longrightarrow d\mathrm{Be}/d\mathrm{O} &\propto \Lambda^n \mathrm{O} \end{aligned} \tag{26}$$

with $nle1$ the index for the scaling law between cosmic ray flux and confinement. If Λ can vary with time—and indeed it is hard to imagine how to avoid such variance—then the simple quadratic relation between Be or B and O is clearly not the prediction of the cosmic ray model. The effect of the variance of Λ is further discussed in the next section.

6 Cosmic Ray Model Dependences

We wish to investigate the dependence of calculated elemental ratios Li/Be and B/Be on various model parameters, for different epochs, i.e. different [Fe/H]. Such a calculation, however, requires specific models for galactic chemical and cosmic ray evolution. Without constructing such models, what we can examine, at a given [Fe/H], are the ratios of production *rates* $d\mathrm{Li}/d\mathrm{Be}$ and $d\mathrm{B}/d\mathrm{Be}$ and their dependence on escape length.

This comparison of production rates provides useful bounds on the elemental ratios any full model would predict. Specifically, at a given epoch [Fe/H] and confinement Λ, $d\mathrm{Li}/d\mathrm{Be}$ gives the value Li/Be would take if the ISM abundances and cosmic ray confinement had been constant for the entire history of the galaxy up to that epoch. The ISM abundances of heavy elements CNO certainly are not constant but build up from zero, while the ISM abundances of H and He do remain roughly constant. The chemical evolution of the ISM affects Li and Be or B differently; Li is largely unaffected, being made mostly by $\alpha + \alpha$ fusion, while Be and B are made by spallation of the CNO targets whose abundances will have always been rising to the levels observed at a particular [Fe/H]. The calculated $d\mathrm{Li}/d\mathrm{Be}$ will thus provide a *lower* bound on the actual Li/Be a full chemical evolution model would predict for a given [Fe/H].[2] The B/Be ratio, however, does not change at all with CNO evolution as long as the C:N:O ratios remain constant, and thus is equal to $d\mathrm{B}/d\mathrm{Be}$. These ratios are roughly constant over the Pop II epoch we consider here, but they do of course change eventually as the O overabundance diminishes to it Pop I value.

[2]Just as the CNO abundances will have changed, so too the cosmic ray flux strength and confinement will have evolved. Though an overall change in flux strength does not affect elemental ratios, evolution in confinement will change the spectrum, with high early confinement leading to a harder spectrum in the past (see next section). This *decreases* the Li/Be ratio, as the $\alpha + \alpha$ production falls off at high energies. This goes in the opposite direction as the chemical evolution effect. However, we will in general explicitly examine the allowed confinement parameters, and in this context we may understand the $d\mathrm{Li}/d\mathrm{Be}$ ratio to be bounded from below.

6.1 Confinement

PCV have detailed a chemical evolution model that can fit observed Be and B data and does produce a slope versus iron that is smaller than the naïve quadratic dependence. In their model, the pathlength is assumed to be larger than the present ~ 10 g cm^{-2}, due to the larger confinement volume of the halo phase versus the disk phase, as well as the larger early gas fraction. They suggested that the confinement varies over the range $10\,\mathrm{g\,cm^{-2}} \lesssim \Lambda \lesssim 1000\,\mathrm{g\,cm^{-2}}$. This variation arises specifically from scaling the escape length as $\Lambda \propto \sigma_g H$; where the gas mass fraction σ_g decreases with time according to the adopted chemical evolution, while the disk scale height H has an exponentially decreasing evolution imposed on it by hand, to simulate the dynamics of the halo collapse.

While this line of reasoning is attractive, one must be cautiously aware of the uncertainties involved. For example, the early behavior of the main confinement mechanism, the galactic magnetic field, is not well understood. The favored means for field generation is through dynamo action tied to the galactic rotation, setting a timescale for generation of $\tau_{rot} \sim 10^8$ yr. Note that in this case the galaxy does not as efficiently retain LiBeB long enough to thermalize them, particularly given the flatter (harder) cosmic ray spectra and/or the inverse kinematics some have suggested (see section 6.2.

Furthermore, Malaney and Butler (1993) have pointed out that the escape length is bounded from above. Physically, this happens when the confinement becomes so large that nuclear destruction of fast LiBeB becomes important. In terms of eq. (1), we have

$$\frac{1}{\Lambda} = \frac{1}{\Lambda_{conf}} + \frac{1}{\Lambda_{nuc}} \tag{27}$$

where $\Lambda_{nuc}^{-1} = \sum_i n_i \sigma_{iA}^{inel} / \rho_{ISM}$. Malaney and Butler note that Λ_{nuc} is species-dependent (whereas Λ_{conf} is not), and they estimate $\Lambda_{nuc} \lesssim 200\,\mathrm{g\,cm^{-2}}$ for protons, thus setting an upper limit for Λ. Prantzos and Cassé (1993) have included this effect in the PCV model and find it makes little change in their results.

What is the affect of a changing confinement? A variation in confinement, acts not only to alter the flux intensity but also to change the shape of the spectrum. This behavior is apparent in figures 2(a) and (b), which plot spectra for different values of confinement. Notice that in both plots the total flux is higher for larger confinement, but by different amounts in different energy regimes. The lowest energy ($\lesssim 100$ MeV/nucleon) portion does not enjoy the same enhancement as the high energy ($\gtrsim 1$ GeV/nucleon) region. One can see in eq. (4) that the spectrum turns over roughly at the energy at which $R(T) \sim \Lambda$. A spectral peak at a larger T means increased power at higer energies. In other words, increasing confinement enhances the highest energy regime and so hardens the spectrum.

Note the different low-energy flux behaviors for the two source types, the forms of which are given explicitly below (section 6.2, eqs. (31) and (32)). The momentum source

diverges as $T \rightarrow 0$, whereas the energy source is finite for small T. These differences manifest themselves in the propagated fluxes. The flux derived from the momentum source has a mild turnover at small energies, and the different Λ fluxes all converge. This behavior is contained in the flux equation (4). At low energy ($T \ll m_p$), the escape length $R(T) \sim T/(\partial T/\partial X) \ll \Lambda$, is slowly varying, and so the exponential in eq. (4) changes slowly as well. On the other hand, the source is a featureless and steeply falling power law: $q(p) \sim p^{-2} \sim T^{-1}$. Thus one can, at sufficiently low energy, ignore the confinement parameter altogether and obtain

$$\phi(T) \approx \frac{1}{w(T)} \int_T^\infty dT' \, q(T') \tag{28}$$

which is independent of confinement. A source power law in total energy, however, the source has a characteristic scale m_p and does not strongly vary over this scale. Since $R(T)/\Lambda$ does change appreciably in this range, eq. 28 is not appropriate, and one must use the full flux equation, with its the strong dependence on confinement. Thus the propagated fluxes do not display the same convergence as those derived from a momentum-law source.

The well-known (e.g. PCV) dependence of the propagated flux on confinement has important consequences for elemental ratios. Although changes in the total cosmic ray intensity will not affect elemental production ratios, spectral changes can. One calculates LiBeB production rates by convolving cross section with flux. Spallation and fusion cross sections generically have low energy resonance peaks up to a few hundred MeV/nucleon, there is a high energy asymptotic behavior characteristic of the interaction. Namely, the cross sections approach a constant at high energies for spallation interactions with a many body final state, but suffer an exponential dropoff for fusion reactions which have few-body final states. (It should be cautioned here that the continued exponential falloff of the $\alpha + \alpha$ fusion reactions above a few hundred MeV is only an extrapolation since no data exists at higher energies; c.f. section 6.3.) Thus the effect on dB/dBe —the ratio of pure spallation products—is to change the emphasis on the resonance region relative to the plateau. Both p and α cross sections for B production have lower thresholds than those for Be, and B cross sections also display higher peaks relative to their plateaus. Consequently, the dB/dBe ratio is lowest at cosmic ray energies in the plateau region. To produce a low B/Be ratio requires a spectrum that gives a larger weight to this energy regime, i.e. a harder spectrum. Just such a spectrum arises from a large confinement scale. The absolute effect on the dB/dBe is small, but important given that B/Be is constrained theoretically and observationally to lie in a small range.

For the dLi/dBe , B production ratio, spectral flattening via large confinement leads to more pronounced changes. The effect again stems from the high energy cross section behavior: while the Be and B cross sections are asymptotically flat, the $\alpha+\alpha \rightarrow Li$ fusion cross sections are assumed to fall off exponentially at high energy. Thus harder spectra have a strong effect dLi/dBe as they emphasize an energy regime where the Li production

is not just reduced relative to Be, but in fact negligible. Thus dLi/dBe strongly decreases with increasing confinement.

We have computed numerically the ratios of rates for the range $10\,\mathrm{g\,cm^{-2}} \leq \Lambda \leq 1000\,\mathrm{g\,cm^{-2}}$. The results appear in figures 3 and 4, and are in agreement with our expectations. The strong dependence of these ratios on the different forms of source spectra will be further discussed below (section 6.2). In reading these figures and comparing to observational data, one must bear in mind the need to include evolutionary effects properly in order to go from the plotted ratios of rates to elemental ratios. Furthermore, as argued above, we see the falloff of both dLi/dBe and dB/dBe at large Λ. Note that the scales in these figures are very different. As Λ is increased from 10 to $1000\,\mathrm{g\,cm^{-2}}$, dLi/dBe falls off by a factor of 10, whereas dB/dBe drops off by only about 15% for the momentum source spectrum and even less so for the energy source spectrum.

In figure 5 we plot the production ratio dLi/dBe against [Fe/H]. Such a plot suggests a comparison with observational data, but bearing in mind the caveat that the dLi/dBe value is only a lower limit to the actual value a full chemical evolution model would give.

In our considerations thus far we have followed most previous work on early LiBeB in putting Λ to be a constant in energy. This parameterization offers a simple way of trying to characterize the early galactic conditions which, as has been pointed out, are poorly understood. While offering simplicity, this approach does suffer the criticism that the choice of a constant escape length does not fit the observed present day cosmic ray pathlength distribution. As shown most recently in Garcia-Muñoz et al. (1987), the escape length varies with energy, increasing slowly to a maximum around a GeV/nucleon, then decreasing as $T^{-0.6}$. They find that their empirical form for $\Lambda(T)$ is well fit by

$$\Lambda(T) = \Lambda_0 \left(\frac{T+m_p}{T_1+m_p}\right)^{\beta} \left[1 - 0.2\exp\left(-\frac{|T-T_1|}{T_2}\right)\right] \tag{29}$$

with $\Lambda_0 = 11\,\mathrm{g\,cm^{-2}}$, $T_1 = 850$ MeV, and $T_2 = 300$ MeV; $\beta = +2$ for $T < T_1$, and $\beta = -0.6$ for $T \geq T_1$. A plot of this function appears in fig. 6. As is well-known, an energy-dependent pathlength changes the solution to the propagation equations (1 and 7), with the replacements

$$R(T)/\Lambda \longrightarrow \int_0^T \frac{dT'}{w(T')\Lambda(T')} \tag{30}$$

where $w(T) = (\partial T/\partial t)/\rho_{ISM} v$.

We have allowed the normalization parameter Λ_0 in $\Lambda(T)$ to vary, and figures 7 and 8 compare the resulting dLi/dBe and dB/dBe to the same ratios obtained with a constant $\Lambda(T) = \Lambda_0$. Note that the changes are relatively small. This is because the energy dependence of the pathlength is most important at high energies, above the region $R(T) \sim \Lambda(T)$ at which the flux turns over. However, the majority of the flux

resides in the region around and below this maximum. Since these energy regimes are largely unaffected, the LiBeB production is weakly affected as well. For the momentum source spectrum the results with and without an energy-dependent pathlength differ by a constant factor of roughly 25%, while for the energy source spectrum the difference varies but is always small $\lesssim 5\%$. The smallness of the difference between the two confinement behaviors justifies the $\Lambda(T) = \Lambda_0$ approximation used in this work and elsewhere. The systematic decrease of the yields for a given scale Λ_0 follows from the energy dependence, under which Λ has a maximum, at $T = T_1$, of only $0.8\Lambda_0$. Thus the confinement is always less than this value, and very much lower for the important low energies.

We have investigated the effect of inelastic nuclear reactions between the primary cosmic rays and the ISM on the effective confinement given in eq. (27). As discussed by Malaney and Butler (1993), this effect contributes an extra species-dependent and energy dependent term to the escape length. Because the pathlength is energy dependent, one must use eq. (30) to compute its effect. We have done so, using cross sections given in Meyer (1972), Townsend & Wilson (1985), and Bystricky, Lechanoine-Leluc, & Lehar (1987). The results appear in Figure 9, and the behavior is as expected. In the usual case, $d\mathrm{Li}/d\mathrm{Be}$ decreases with increasing $\Lambda_{eff} = \Lambda_{esc}$, and we now have $\Lambda_{eff} < \Lambda_{esc}$. Thus, we expect $d\mathrm{Li}/d\mathrm{Be}$ to be consistently larger at a given Λ_{esc}, as is the case. This effect is more pronounced at high Λ_{esc}, where the nuclear loss term dominates.

Another property of the early galaxy with bearing on confinement is the state of ionization of the ISM. Energy losses are increased in an ionized medium, leading to a shorter ionization range. Because the confinement always appears as R/Λ (for $\Lambda(T)$ constant in energy), this effectively increases the escape length PCV account for ionization by doubling the energy losses for neutral media, a procedure which amounts to assuming a fully ionized medium (Ginzburg & Syrovatskii 1964). If indeed the ionization state evolves during the Pop II epoch, the effective change in Λ can affect the cosmic ray spectrum independent of the considerations in eqns. (27) and (30).

6.2 Spectrum

Both WSSOF and PCV have independently argued for a flatter spectrum in early cosmic rays than that presently observed. The key observation supporting this argument is the B/Be ratio. Although the observational uncertainty here is clearly large, the current preliminary numbers are low compared to the present day observed value of 15 ± 3 (with e.g. Mathews, Walker, and Viola (1985) predicting $\simeq 17$ for Pop I), and to the Pop II value of $\simeq 14$ calculated in WS (using a transported spectrum $\phi(T) \propto (T + m_p)^{-2.7}$), and Pop I C:N:O ratios.

The argument for a flat early cosmic ray spectrum arises if one takes a low central value for the Pop II B/Be ratio seriously. (Remember values below 7 are impossible in any spallation model, and so far hypothetical stellar processes enhance B.) Be and

B arise from the same spallation processes, so there are a limited number of available differences to exploit in fixing the ratio. Their differences in mass and charge lead to different ionization losses and ranges, and consequently different confinement for the two elements (at a given energy per nucleon). However, with the ionization ranges scaling law of eq. (5), it is clear that $R_B(T) < R_{Be}(T)$, and thus energy loss and thermalization effects (c.f. eq. 8) favor B rather than Be and so act to *increase* the B/Be ratio. The other important difference between Be and B production rates lies in their spallation cross sections. As argued in section 6.1, the differences make the B/Be ratio sensitive to the cosmic ray spectrum, with a lower B/Be for flatter spectra.

Another argument for a flatter spectrum has been offered by PCV (but weakened by Malaney and Butler's (1993) arguments; see Prantzos & Cassé (1993)). PCV note that the low observed Li/Be ratio (once the primordial Li component has been subtracted) is more easily reproduced by a flat spectrum because of exponential dropoff of $\alpha + \alpha$ cross sections.

In addition to the effect of changes in the confinement, the propagated spectrum obviously depends on the source spectrum. PCV choose as a source spectrum a power law in momentum, $q(p) \propto p^{-2}$, a type of spectrum appearing in models of cosmic ray shock acceleration. Such models assume acceleration via scattering off of supernova shock waves, and have been successful in reproducing galactic and heileospheric spectra in detail (c.f. the Blanford & Eichler (1987) review). Note that the PCV spectral index of 2 is the universal limiting value for very large Mach number shocks. We note, however, that despite the success of and active interest in this model, there remains disagreement upon the the appropriate model for acceleration. It is thus worthwhile to examine the sensitivity of the LiBeB yields to the assumed spectrum, where there remains some flexibility to choose the spectral index.

Most important for LiBeB production is the choice of spectral type. While shock acceleration models suggest source power laws in magnetic rigidity and hence momentum are good candidates, the measured (and hence propagated) cosmic ray flux at earth is also consistent with a source spectrum in total energy per nucleon. The two are of course difficult to distinguish at the relativistic energies at which the cosmic ray measurements are unaffected by solar modulation effects. Furthermore, solar effects introduce large uncertainties at lower energies, rendering unreliable the data that could make this distinction. In addition, a power law in total energy has the advantage that it remains finite at low energies, thus providing a mockup of physical processes responsible for preventing a divergence in the source at low energies.

Thus we have tried source spectra of power laws both in momentum and in total energy per nucleon, i.e.

$$\begin{aligned} q(p) &\propto p^{-\gamma} \\ &\Longrightarrow q(T) \propto (T+m_p)(2m_pT+T^2)^{-(\gamma+1)/2}\ , \text{ and} \qquad (31) \\ q(T) &\propto (T+m_p)^{-\gamma} \qquad (32) \end{aligned}$$

with m_p the proton mass. For the shock acceleration model–inspired momentum spectrum, the index γ is given by

$$\gamma \approx \left(2 + \frac{4}{M^2}\right) \tag{33}$$

for the case of large Mach number $M = v_{shock}/c_{sound}$, the ratio of shock velocity to the sound speed in the shocked gas. Note that the Mach number depends upon the local ISM sound speed, which in turn depends upon, e.g. the ISM density and pressure. If the early galaxy, or its primordial protogalactic building blocks, were to be significantly hotter or denser than today, then potentially the cosmic ray spectrum could be quite different.

For the total energy spectrum we take $\gamma = 2.7$, which is consistent with the measured, transported cosmic ray spectrum. Note however, that this choice is inappropriate for the simple leaky box with energy dependent escape length. In this case, we live in the confinement region (the galaxy), and so the escape energy dependence is folded into that of the source. The proper source index is thus $\gamma_{source} = \gamma_{obs} - \beta \approx 2.1$, with β the high-energy index of the energy-dependent Λ from eq. (29). This is not the case in, for example, the nested leaky box model, in which we do not live in the confinement region (which shrouds the sources), and so we do not see its energy dependence: $\gamma_{source} = \gamma_{obs}$. Again, the model uncertainty argues for examination of a range of source indices.

Note the dramatic effect on the Li/Be and B/Be plots (figs. 3 and 4). The large low energy flux of the momentum spectrum makes this spectrum softer than one in total energy, and the resulting elemental ratios behave as one would expect for such a soft spectrum. As discussed above in section 4, low energy resonance behavior is emphasized and leads to large Li/Be and B/Be ratios.

We have allowed the spectral index γ to vary over the range $2 \leq \gamma \leq 3$. Results appear in figures 10 and 11 from which it is apparent that the LiBeB production rates from a source with a momentum spectrum are more sensitive to changes in spectral index than are the rates for a source total energy law. Indeed it is clear from fig. 10 that for source spectra in momentum, indices with $\gamma \gtrsim 2.5$ lead to Li-to-Be relative production rates in ratios approaching 10^3. This is clearly undesirable given that all observed Be abundances are $\gtrsim 10^{-13}$, thus implying associated Li production larger than the observed plateau, even without the large primordial Li component.

While the relative B and Be rates (figure 11) do not vary as dramatically for the momentum spectrum, here too they are much more sensitive than the same ratios given a total energy spectrum. Additionally, the same range of indices that overproduce Li relative to Be give the largest values for B relative to Be as compared to low values for the current preliminary but uncertain data. Nevertheless, it is intriguing that the range of indices that fail for the Li to Be ratio seem to also do the worst for B to Be. Thus momentum spectra with indices steeper than about 2.5 are less favored at the present time. Note that we get no such constraints for source spectra in total energy, as we see only mild sensitivity to a source index for Li to Be (for which all values are completely

acceptable), and completely insensitivity for B to Be.

In figure 12 we plot $d\mathrm{Li}/d\mathrm{Be}$ vs Λ, as in figure 3, but with different spectral indices. For each spectral type, the production ratio grows with the steepness of the spectrum, the growth being more pronounced for the scale-free momentum law. Figure 13 is a similar plot for the $d\mathrm{B}/d\mathrm{Be}$ ratio. Note that this ratio is mildly sensitive to the momentum spectral index, which can change $d\mathrm{B}/d\mathrm{Be}$ by 1 to 2 units, i.e. 10-20%. Such a change might be detectable as observations improve. The $d\mathrm{B}/d\mathrm{Be}$ ratio is even less sensitive to the index of a source with a total energy spectrum. The change over the whole range is of order 5%.

As we have alluded to earlier, a direct comparison of the data and the model calculations given here is extremely difficult but can be suggestive. The ratio of of Li/Be given in table 1 contains the primordial Li component as well as the cosmic-ray produced Li. In some cases this correction might be quite large (a factor of 10 or more) so that the ratios in the table represent extreme upper limits. If we had a specific cosmic-ray nucleosynthesis model, one could, as shown in Olive and Schramm (1992) extract a Big Bang Li abundance. For the cosmic-ray nucleosynthesis model used in WSSOF this led to a value $[\mathrm{Li}]_{BB} = 2.01 \pm 0.07$, however as we can see from figures 5*a* and 5*b*, there is significant model dependence in the Li/Be ratio. Also, the absolute [Li] values are plagued by the poorly given systematic errors mentioned in sectios 2. Furthermore, as we have also noted, the element ratio will also be affected by chemical evolution. Thus one can with certainty only require the data points as given in the table to lie above any model curve in the figures. The trend in the data is also seen in the figures, ie. at high metallicities the Li/Be ratio is smaller. Note that a large primordial subtraction would favor the lower ratios found with the cosmic-ray energy source spectrum.

To get a feeling for the comparison between data and these models, we can make a primordial subtraction corresponding to $[\mathrm{Li}]_{BB} = 2.0$. It hard to make the primordial ^{7}Li abundance much smaller (Walker et al 1993; Krauss & Romanelli, 1990) and if it were much larger there would be no room for cosmic-ray produced Li. In Figure 14 we show the values of Li/Be with the above primordial subtraction. Error bars are too large to display. We also plot the ratio from the energy and momentum-spectra for $\Lambda = 100\,\mathrm{g\,cm^{-2}}$ as a function of [Fe].

6.3 Other Model Features

The conventions for reporting spallation/fusion cross sectional data are strictly speaking incomplete for calculations of LiBeB production, and thus require a model to make some assumption regarding the kinematics of these interactions. Specifically, the tabulated data and semi-empirical fits give the *total* cross section for LiBeB production at a given incident energy. As seen explicitly in eq. (2), however, we require the full, *differential* cross section $d\sigma_{ij}^{A}/dT_{LiBeB}\,(T_{LiBeB}, T_{CR})$. Meneguzzi et al. (1971) and many subsequent authors address this issue by assuming that the differential cross section is very sharply

peaked around those values of the LiBeB energy for which $T_{LiBeB} = T_{CR}$. They put

$$\frac{d\sigma_{ij}^{A}}{dT_{LiBeB}}(T_{LiBeB}, T_{CR}) = \sigma_{ij}^{A}(T_{CR})\ \delta\left(T_{LiBeB} - T_{CR}\right)\ . \tag{34}$$

with $\sigma_{ij}^{A}(T_{CR})$ the tabulated cross section.

While the approximation of sharp peaking over a small range of product energies appears to be borne out experimentally in the cases where it has been checked, the other approximation, that of equal energies (per nucleon) in the initial and final state is only valid for the case of heavy cosmic rays on light targets. We have relaxed the latter assumption, allowing for the CR energy to be related to the LiBeB energy via some function $E_f(T_{CR})$, changing eq. (34) to

$$\frac{d\sigma_{ij}^{A}}{dT_{LiBeB}}(T_{LiBeB}, T_{CR}) = \sigma_{ij}^{A}(T_{CR})\ \delta\left(T_{LiBeB} - E_f(T_{CR})\right)\ . \tag{35}$$

With this more general formalism we have investigated two possible kinematic behaviors. One ansatz is that in the center of momentum frame the LiBeB is produced at rest, with the lighter debris moving in such a way as to conserve energy. This is the assumption we have made throughout this paper. One should compare this to another common assumption that in the frame in which the light target is at rest, the kinetic energy per nucleon of the daughter nucleus is the same as that of the heavy CR parent. We have plotted the dLi/dBe ratio for these two cases in figure 15.

The issue of spallation kinematics is raised if one considers an alternative to the usual production scenario we have presented so far. Duncan et al. (1992) and PCV both attempt to address the question of the Be vs Fe slope with the suggestion that perhaps most of the LiBeB production is not from light (p, α) cosmic rays on heavy (CNO) ISM nuclei, but the reverse: heavy cosmic rays on light ISM nuclei. Furthermore, if the heavy cosmic rays do not have the ISM abundance or something near to it, then this could yield significantly different Be and B production. Increased cosmic ray heavies would result, for example, if supernovae were to accelerate their own ejecta. The evidence is not definitive on this issue, but there are possible problems in maintaining consistency with an assumed first ionization potential dependence of the cosmic ray source abundances.

At any rate, we have investigated the dependence of the spallation yields on forward, reverse kinematics. Figure 16 compares the dLi/dBe ratio for the cases of normal kinematics (i.e. LiBeB synthesis primarily from light CR on heavy ISM with a small admixture of the reverse) to reverse kinematics, in which we assume $y_{CNO}^{CR} \approx y_{CNO}^{solar}$, and thus dominate the LiBeB production. Note that here the dLi/dBe ratio is much smaller, as the $\alpha + \alpha$ process is not as dominant as in the usual early galactic case.

Note that, in considering the thermalization of LiBeB, authors from Meneguzzi et al (1971) to PCV apparently use $S \equiv 1$ over all energies in the case of light cosmic rays on heavy targets. These authors note that the daughter nuclei move more slowly than the

cosmic ray parent and so are likely to be stopped. However, as we are considering cases where the flux can be very hard, then we may still have quite energetic daughter nuclei and it is important to properly allow for incomplete stopping. Note that Li, which is made primarily by $\alpha + \alpha$ fusion, is thus the only spallogenic element we consider for which (in the dominant production process) the cosmic ray projectile not much lighter than the ISM target. Consequently, the Li will be the fastest daughter nuclei, and thus accurate treatment of trapping is particularly important. To compare with previous work, we have computed yields with $S \equiv 1$ for both kinematics. Results appear in figure 17.

We see in figure 17 that the direction of the effect depends upon the spectral type. For a momentum source, one gets a higher dLi/dBe ratio when allowing for realistic trapping of LiBeB. The change, ranging from about 40% at large Λ down to 10% at small ones, arises because Be production at high energy exceeds that of Li (because of the $\alpha+\alpha$ falloff at high energy), and these high energy Be are less likely to be thermalized than slower daughters. This is not the whole story for a source law in energy. Here, the spectral peak is much more pronounced and at a high energy ($\sim m_p$) than the (lower energy) peak of the flux from the momentum source. The flux from the energy source thus *rises* steeply at the ($\sim 100 MeV$) dropoff in the Li production cross sections. Consequently, the majority of Li production occurs in the beginning of the high energy tail of the cross section. By disfavoring the high energy products through incomplete stopping, one removes the faster Li made at the highest overlap of cross section and flux. With $S = 1$, however, these fast daughters are included and so raise the Li production relative to Be.

Let us now look at the dependence of the dLi/dBe production rate on the asymptotic value of cross section for $\alpha+\alpha \rightarrow {}^{6,7}$Li. This is a fusion process and is physically different from the other spallation processes. The data shows that these cross sections decrease exponentially with energy, although the highest energy at which a definite cross section has been reported is only about 50 Mev/nucl. Evidence for the continued dropoff comes instead from upper bounds to the cross sections, which go out to $\sim$ 200 MeV/nucl, with no plateau detected. While Read and Viola (1984) recognize this, they suggest in their cross section tabulation that a plateau might nevertheless eventually be found to exist, and some work (notably PCV) has employed such a feature, although the data does not justify such an assumption. We have examined the Li/Be ratio with and without such a plateau, and find that it can have a significant effect, particularly for cases of large confinement or spectral index near 2, as these emphasize the high energy events in which the differences are important. Figure 18 compares the dLi/dBe ratio with and without the cross section plateau. While the differences are not large for a momentum source ($\lesssim 10\%$), for a source power law in total energy, the effect is about a factor of 2. Since we see no evidence as yet for a plateau, in all our other computations none is assumed to exist. However, as the effect of such a plateau is significant, we feel it is very important

for experiments to investigate the behavior of the $\alpha + \alpha \rightarrow {}^{6,7}\mathrm{Li}$ at high energy.

Finally, we note the important but not decisive contribution to the overall uncertainty of experimental uncertainties in cross sections and in energy losses. Cross section uncertainties are typically at a level of $\delta\sigma/\sigma \simeq 10 - 20\%$. While these errors are large enough to be significant, they clearly are smaller than the other model effects we have noted above, consequently making the model choices important ones. Energy losses are better known, with $\delta b/b \simeq \delta R/R \simeq 5\%$ at low energies (where they are unimportant), and $\lesssim 2\%$ at higher energies. These errors do not significantly contribute to our overall uncertainty.

7 Gamma Ray Production

The same passage of cosmic rays through the ISM that produces LiBeB must also create γ-rays, as noted by Silk and Schramm (1993), Fields, Schramm and Truran (1993), and Prantzos and Cassé (1993). The primary γ-ray source from the nuclear cosmic ray component[3] arises from inelastic scattering of cosmic rays on the ISM, with $p + p \rightarrow \pi^0 \rightarrow 2\gamma$. Thus the γ-ray spectral peak is around $m_\pi/2$.

The total (isotropic) γ-ray production rate by the nuclear component of the cosmic rays, per second per cubic centimeter, is given by

$$\Gamma = n_H \int_{T_{th}}^{\infty} dT \phi_p(T) \sigma_{pp}^{\gamma}(T) \tag{36}$$

in an obvious notation. Note that the calculation is similar to that for LiBeB production. Indeed this process occurs under very similar conditions to Li production, as both processes derive from reactions between protons and α nuclei, which in the early galaxy are undepleted both in the cosmic rays and in the ISM. Thus we may expect to scale the γ-ray production to that of Li via $\sigma(\alpha + \alpha \rightarrow \mathrm{Li})$ to the $\sigma(p + p \rightarrow \gamma)$ cross section ratio. One should note, however, that such a simple scaling ignores the different energy dependences of these processes, and ignores the issue of the incomplete trapping of the Li fusion products.

Because γ-ray production so closely follows that of Li, the model dependences will be similar. In particular, the effects of cosmic ray evolution will be similar, as will the uncertainties in scaling the γ-ray production to the Be. In a subsequent paper on specific galactic evolution models we intend to quantify the γ-fluxes and use them as a complementary probe to the LiBeB abundance behaviors described here.

[3]As opposed to the cosmic ray electrons, which produce lower energy γ-rays by brehmsstrahlung. We do not explicitly consider the electron component here, but Prantzos and Cassé argue that it should scale with the nuclear component as it does today, and using this scaling they calculate the contribution to the isotropic γ-ray background.

8 Conclusions

In this paper we showed in detail that there are many uncertainties about early cosmic ray behavior and therefore a range of possible assumptions from which one must choose in building a model for this behavior. Furthermore, the variance in possible early cosmic ray models can have a significant effect of on the calculation of cosmic ray production of LiBeB (and γ-rays) in the early galaxy. The variance in the models derives both from uncertainties about present cosmic rays and from uncertainties about the evolution of their injection and acceleration, as well as confinement.

Because these uncertainties are difficult to resolve, we conclude that future work in modeling early cosmic rays must allow for cosmic ray model variances and evolution. As shown in section 6.2, the choice of source spectral type is significant yet not settled even for today's cosmic rays, with power laws both in total energy per nucleon and in momentum being allowed. Also, we show that cosmic ray evolution derives not only from changes in source strength, but also from changes in confinement, as detailed in sections 4 and 6.1. Evolution of confinement can have important effects, for example in altering the naïvely expected Be-to-Fe slope, as outlined here and shown in the detailed model of PCV. Additional considerations are noted in section 6.3, most notably the effects of inelastic nuclear collisions on confinement, as have been noted by Malaney and Butler (1993).

In light of our findings we now turn to the work to date on early cosmic ray production of LiBeB, namely the relatively model-independent work of WSSOF and its sequels, and the detailed cosmic ray and chemical evolution model of PCV. The flatness of the curves in figure 13 justifies the claim in WSSOF that the B/Be ratio in cosmic ray models is indeed insensitive to the details of cosmic ray models. In addition, because Be and B are pure spallation (as opposed to $\alpha + \alpha$ fusion) products, their production ratio $d\mathrm{B}/d\mathrm{Be}$ is independent of [Fe/H] and varies only with the C:N:O ratios of targets. To the extent that this ratio remains fairly constant, we can conclude that the B/Be ratio is insensitive to chemical evolution as well, and thus. We consequently find B/Be to be well-chosen as a model-independent signature of the spallation process.

The Li isotopic ratio, discussed in SFOSW, $^6\mathrm{Li}/^7\mathrm{Li}$ shows a similar independence to cosmic ray model features but does have a moderate sensitivity to chemical evolution via the ISM ratio He/CNO, which sets the relative contributions of the $\alpha + \alpha$ fusion versus spallation contributions to $^6\mathrm{Li}/^7\mathrm{Li}$. We find that $d^7\mathrm{Li}/d^6\mathrm{Li}$ is always within $\sim 30\%$ of unity for all spectra and escape parameters considered here. This uncertainty is much smaller than that of the $^6\mathrm{Li}/^7\mathrm{Li}$ ratio of Smith et al (1992). Consequently we find SFOSW's assumption of a temporally constant $d^6\mathrm{Li}/d^7\mathrm{Li}$ production ratio to be appropriate.

However, we find that the "zeroth order model" of WS, SFOSW, and SFOSW to be overly simplistic not only in its lack of chemical evolution, but also in its lack of any kind of cosmic ray evolution. The effect on predictions of this model is unimportant for

the B/Be limits, but their calculations of the Li/Be ratio are, as we have noted, only a lower bound to the actual ratios.

The PCV model does allow for chemical as well as cosmic ray evolution, and in particular they allow for evolution of cosmic ray confinement. We thus find their model indeed to be a useful examination of LiBeB production. Our caution is that their model is a specific one made with particular, albeit reasonable, assumptions. Their specific cosmic ray source model we find to be well-motivated and reasonable, but not a unique choice and we would urge that future work consider different momentum source indices, as well as source spectra in total energy. Furthermore, PCV admit that their particular implementation is to some degree arbitrary. In the first place, it is not obvious which parameters control Λ. Secondly, even given a particular scaling prescription, it is not trivial to model the input parameters (e.g. galactic scale height and magnetic field) accurately. PCV assume Λ depends upon the scale height of the collapsing disk, but they do not compute the collapse explicitly, and so impose an *ad hoc* time dependence. Clearly a firm model for Λ evolution is crucial, but at present is unavailable. We agree with PCV that more theoretical work in this area is needed.

In summary, we feel that improved data on PopII LiBeB abundances with consistent controls on systematics might lead to an ability to constrain models for the origin and propagation of cosmic rays in the early galaxy.

We thank Doug Duncan, Gary Steigman, Simon Swordy, Mike Thayer, Julie Thorburn, and Terry Walker for useful discussions. This work was supported in part by the DOE (at Chicago and Fermilab), by NASA and NSF at Chicago, and by NASA through NAGW-2381 (at Fermilab). This work was also supported in part by DOE grant DE-AC02-93ER-40105 at Minnesota. The work of KAO was in addition supported by a Presidential Young Investigator Award.

References

Asakimori, K., et al 1993, in Proc. of the 23rd Int. Cosmic Ray Conf. (Calgary), 2, 25

Blanford, R., and Eichler, D. 1987, Phys Reports, 154, 1

Boesgaard, A.M., & King, J. 1993, preprint

Bystricky, J., Lechanoine-Leluc, C., & Lehar, F. 1987 J. Physique, 48, 199

Buckley, J., Dwyer, J., Müller, D., Swordy, S., and Tang, K.K. 1993, ApJ submitted

Ceasarsky, C.J. 1980, ARAA, 18, 289

Ceasarsky, C.J. 1987, in Proc. of the 20th Int. Cosmic Ray Conf. (Moscow), 8, 87

Dearborn, D.S.P., Schramm, D.N., Steigman, G., & Truran, J. 1988 ApJ 347, 455

Duncan, D.K., Lambert, D.L., & Lemke, M. 1992 ApJ, 401, 584

Feltzing, S., & Gustaffson, B. 1993, ApJ submitted

Fields, B. D., Schramm, D. N., & Truran, J. W. 1993 ApJ, 506, 559.

Garcia-Muñoz, M., Simpson, J.A., Guzik, T.G., Wefel, J.P., & Margolis, S.H. 1987 ApJS 64, 269

Gilmore, G., Edvardsson, B., & Nissen, P.E. 1992a, AJ, 378, 17

Gilmore, G., Gustafsson, B., Edvardsson, B., & Nissen, P.E. 1992b, Nature, 357, 379

Ginzburg, V.L., & Syrovatskii, S.I. 1964 The Origin of Cosmic Rays, (Pergamon: New York), 121

Hobbs, L.M., & Duncan, D., 1987, AJ, 317, 796

Hobbs, L.M., & Thorburn, J.A., 1991, ApJ, 375, 116

Janni, J.F. 1982, Atomic Data & Nuc Data Tables, 27, 34

Krauss, L.M., & Romanelli, P. 1990 ApJ, 358, 47

Malaney, R.A., & Butler, M.N. 1993, CITA preprint 92/26

Meneguzzi, Audouze, J., & Reeves, H. 1971 A&A, 15, 337

Meyer, J.P. 1972 A&ASup, 7, 417

Molaro, P., Castelli, F., & Pasquini, L. 1993, Origin and Evolution of the Light Elements, ed. N. Prantzos, E. Vangioni-Flam, & M. Cassé (Cambridge: Cambridge University Press), 153

Northcliffe, L.C., & Schilling, R.F. 1970, Nuc Data Tables A7, 233

Olive, K. A., & Schramm, D. N. 1993 Nature, 360, 439

Olive, K.A., Prantzos, N., Scully, S., & Vangioni-Flam, E. 1993, ApJ in press

Pilachowski, C.A., Sneden, C., & Booth, J. 1993, ApJ, 407, 699

Prantzos, N. 1992, in Nuclei in the Cosmos, ed. F. Kappeler & K. Wisshak (Philadelphia:IOP Publishing) 471

Prantzos, N., & Cassé, M. 1993 Saclay preprint

Prantzos, N., Cassé, M., Vangioni-Flam, E. 1993 ApJ, 403, 630 (PCV)

Read, S.M., & Viola, V.E., 1984

Rebolo, R., Molaro, P., Abia, C., & Beckman, J.E. 1988a A&A, 193, 193

Rebolo, R., Molaro, P., & Beckman, J. 1988b, A&A, 192, 192

Reeves, H., Fowler, W. A., & Hoyle, F. 1970 Nature 226, 727

Ryan, S., Bessel, M., Sutherland, R., & Norris, J. 1990, ApJ, 348, L57

Ryan, S., Norris, J., Bessel, M., & Deliyannis, C. 1992 ApJ, 388, 184

Silk, J., & Schramm, D.N., 1993, ApJ, 393, L9

Smith, V.V., Lambert, D.L., & Nissen, P.E. 1992, ApJ, 408, 262

Spite, F., Maillard, J.P., & Spite, M. 1984, A&A, 141, 56

Spite, F., & Spite, M. 1982, A&A, 115, 357

———. 1986, A&A, 163, 140

Steigman, G., Fields, B. D., Olive, K. A., Schramm, D. N., & Walker, T. P. 1993 ApJ, 415, L35 (SFOSW)

Steigman, G., & Walker, T. P. 1992 ApJ, 385, L13 (SW)

Thomas, D., Schramm, D.N., Olive, K.A., & Fields, B.D. 1993, ApJ, 406, 569

Townsend, L.W., & Wilson, J.W. 1985, Tables of Nuclear Cross Sections for Galactic Cosmic Rays, NASA Ref Pub 1134

Walker, T. P., Mathews, G. J., & Viola, V. E. 1985 ApJ 299, 745

Walker, T. P., Steigman, G., Schramm, D. N., Olive, K. A., & Fields, B. D. 1993 ApJ, 413, 562 (WSSOF)

Walker, T. P., Steigman, G., Schramm, D.N., Olive, K.A., & Kang, H. 1991, ApJ, 376, 51

Woosley, S.E., Hartmann, D.H., Hoffman, R.D., & Haxton, W.C. 1990, ApJ, 356, 272

FIGURE CAPTIONS

Figure 1: (*a*) The cosmic ray proton flux and α spectra ϕ compared to source spectra ($q(p) \propto p^{-2}$) scaled as Λq. Note that in the limit of no energy losses (a good approximation at high energy) we have $\phi = \Lambda q$, and so departure from this scaling indicates the effect of energy losses. Note also that the α flux scales very well with the proton flux as the He cosmic ray abundance 0.08. That this proportionality is accurate over the whole energy range reflects the similar energy loss behavior due to the scaling A/Z^2.

(*b*) As in (*a*), for $q(T) \propto (T + m_p)^{-2.7}$.

Figure 2: (*a*) The transported cosmic ray proton flux for a range of confinement parameters: Λ = 10, 30, 100, 300, and 1000 g cm^{-2}. The source is a power law in momentum, $q(p) \propto p^{-2}$.

(*b*) As in (*a*), for a source power law in total energy, $q(T) \propto (T + m_p)^{-2.7}$.

Figure 3: The Li to Be production ratio as a function of pathlength. The solid line is for a source spectrum that is a power law in momentum, $q(p) \propto p^{-2}$; the dashed line is for a source power law in total energy, $q(T) \propto (T + m_p)^{-2.7}$. We put [C/H] = [N/H] = -2.5, [O/H] = -2.0.

Figure 4: The B to Be ratio as a function of pathlength, plotted as in fig. 3.

Figure 5: (*a*) The production ratio of Li to Be as a function of metallicity [Fe/H], for a source $q(p) \propto p^{-2}$, and for a range of conement parameters: Λ = 10, 30, 100, 300, and 1000 g cm^{-2}. See discussion in the text regarding comparison to observations.

(*b*) As in (*a*), for a source $q(T) \propto (T + m_p)^{-2.7}$.

Figure 6: A plot of the pathlength distribution of equation (29), chosen in Garcia-Muñoz et al. (1987) to provide the best fit to the observed B/C ratio.

Figure 7: (*a*) The dLi/dBe ratio for $\Lambda(T) = \Lambda_0$ (solid line), and for $\Lambda(T)$ given by equation (29), with Λ_0 as indicated on the figure (broken line). The source spectrum is $q(p) \propto p^{-2}$, and ISM abundances are [C/H] = [N/H] = -2.5 and [O/H] = -2.0.

(*b*) As in (*a*), for a source spectrum $q(T) \propto (T + m_p)^{-2.7}$.

Figure 8: (*a*) The dB/dBe ratio for $\Lambda(T) = \Lambda_0$ (solid line), and for $\Lambda(T)$ given by equation (29), with Λ_0 as indicated on the figure (broken line). The source spectrum is $q(p) \propto p^{-2}$ and ISM abundances are [C/H] = [N/H] = -2.5 and [O/H] = -2.0.

(*b*) As in (*a*), for a source spectrum $q(T) \propto (T + m_p)^{-2.7}$.

Figure 9: (*a*) The $d\mathrm{Li}/d\mathrm{Be}$ ratio for $\Lambda = \Lambda_{esc}$, the usual case (solid line), and for $\Lambda(T)$ given by eq. (27), (broken line), where we have plotted against Λ_{esc}. The source spectrum is $q(p) \propto p^{-2}$ and ISM abundances are [C/H] = [N/H] = -2.5 and [O/H] = -2.0.

(*b*) As in (*a*), for a source spectrum $q(T) \propto (T + m_p)^{-2.7}$.

Figure 10: The ratios of Li to Be production rates, shown as a function of source spectral index γ for a source spectrum in momentum and in total energy. Note that the yields from the momentum spectrum are very sensitive to the index adopted, and the ratio of rates can become unacceptably high in this case. In contrast, the yields from the total energy spectrum are relatively insensitive to spectral index, and are all at acceptably low levels.

Figure 11: As in fig. 10 for the ratio of B to Be rates; the same trends are seen. Note however that the B/Be ratio is negligibly sensitive to the total energy index, and is only mildly sensitive to that for the momentum law.

Figure 12: (*a*) Curves of $d\mathrm{Li}/d\mathrm{Be}$, as a function of Λ, for different spectral indices γ. The source is $q(p) \propto p^{-2}$.

(*b*) As in (*a*), for $q(T) \propto (T + m_p)^{-2.7}$.

Figure 13: As in fig. 12, for the $d\mathrm{B}/d\mathrm{Be}$ ratio.

Figure 14: Similar to figure 5. We plot $d\mathrm{Li}/d\mathrm{Be}$ for each source type at $\Lambda = 100\,\mathrm{g\,cm^{-2}}$. The data, as described in the text, has been corrected assuming the minimal allowed primordial ^{7}Li production, $[^7\mathrm{Li}]_{BB} = 2.0$ and thus (linearly) subtracting this amount from the Li vales of table 1. See discussion in the text regarding caveats in comparing the theoretical curves, which are upper bounds, to the data.

Figure 15: The $d\mathrm{Li}/d\mathrm{Be}$ ratio for different determinations of the daughter nucleus kinematics. The solid curve is calculated assuming that the daughter nucleus is stationary in the center of momentum frame of the parents; this is the standard used throughout this paper. The dashed curve is calculated assuming that, in the rest frame of the light parent, the daughter kinetic energy per nucleon is equal to that of the heavy parent. The source spectrum is $q(p) \propto p^{-2}$ for curves (*a* and (*b*, and $q(T) \propto (T + m_p)^{-2.7}$ for curves (*c* and (*d*. Additionally, we put [C/H]=[N/H]=-2.5, [O/H]=-2.0.

Figure 16: (*a*) The $d\mathrm{Li}/d\mathrm{Be}$ ratio for (solid line) cosmic ray CNO abundances equal to ISM abundances ($y_{CNO}^{CR} = y_{CNO}^{ISM}$, the usual case), and for (dashed line) cosmic ray CNO abundances fixed to be solar ($y_{CNO}^{CR} \gg y_{CNO}^{ISM}$). The source spectrum is $q(p) \propto p^{-2}$ and ISM abundances are [C/H] = [N/H] = -2.5, and [O/H] = -2.0

(*b*) As in (*a*), for a source spectrum $q(T) \propto (T + m_p)^{-2.7}$.

Figure 17: The $d\mathrm{Li}/d\mathrm{Be}$ ratio with incomplete LiBeB trapping, i.e. with $S_{\mathrm{LiBeB}} = \exp(R/\Lambda)$ (solid line), and with complete LiBeB trapping ($S_{\mathrm{LiBeB}} = 1$). The source spectra are as labeled, and we put and [C/H]=[N/H]=-2.5, [O/H]=-2.0.

Figure 18: (*a*) The $d\mathrm{Li}/d\mathrm{Be}$ ratio in the absence (solid line) and presence (broken line) of a high energy plateau in the $\alpha + \alpha \rightarrow {}^{6,7}\mathrm{Li}$ cross section. The source spectrum is $q(p) \propto p^{-2}$ and ISM abundances are [C/H] = [N/H] = -2.5 and [O/H] = -2.0. Note the small ($\sim 10\%$) increase with the plateau.

(*b*) As in (*a*), for a source spectrum $q(T) \propto (T + m_p)^{-2.7}$. Here the difference is larger (a factor of ~ 2), as the flux is harder than that from the momentum flux, and so the high energy cross section behavior is more important.

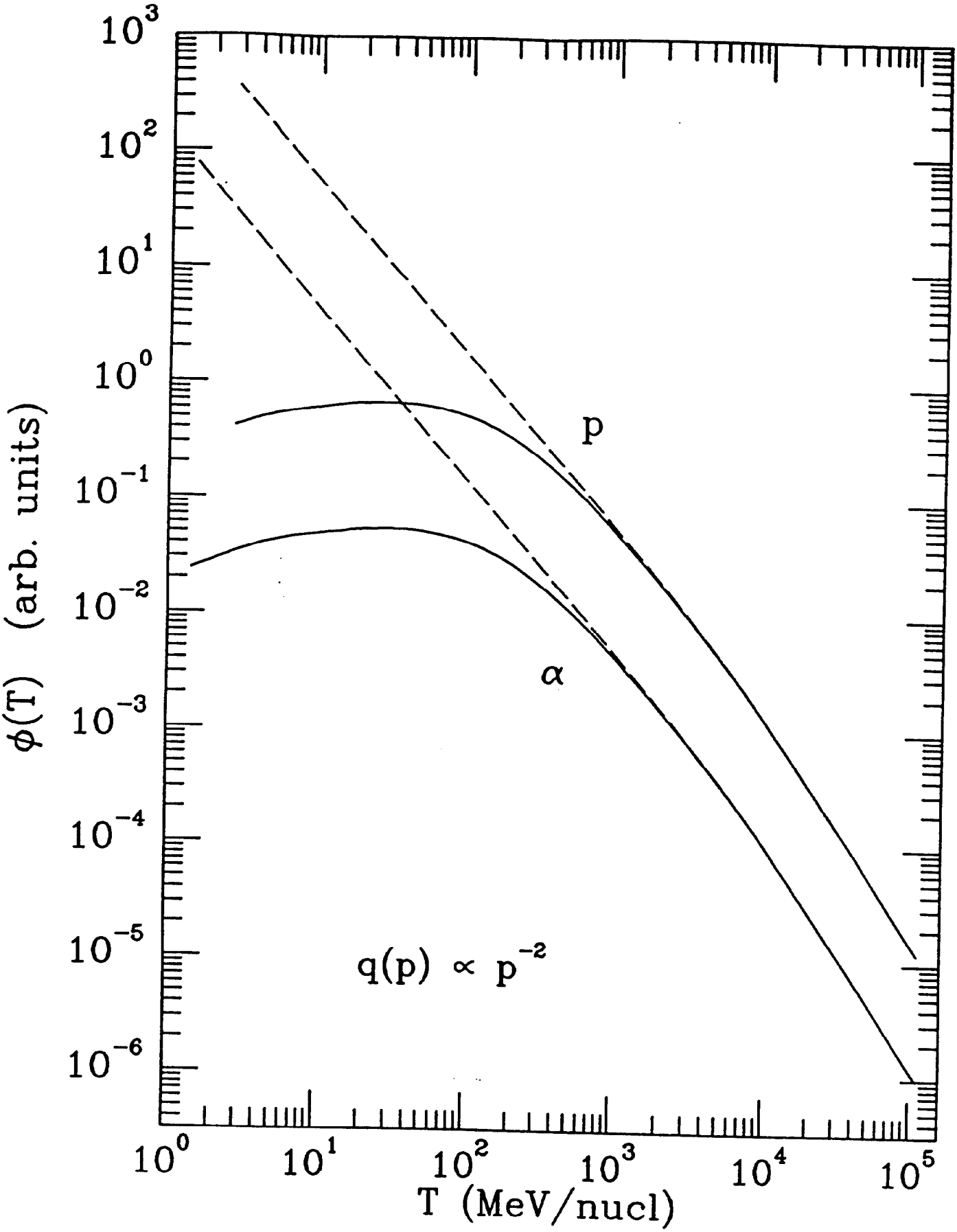
10^3
10^2
10^1
10^0
10^{-1}
10^{-2}
10^{-3}
10^{-4}
10^{-5}
10^{-6}
$\phi(T)$ (arb. units)
p
α
$q(p) \propto p^{-2}$
10^0
10^1
10^2
10^3
10^4
10^5
T (MeV/nucl)

FIG 1 (a)

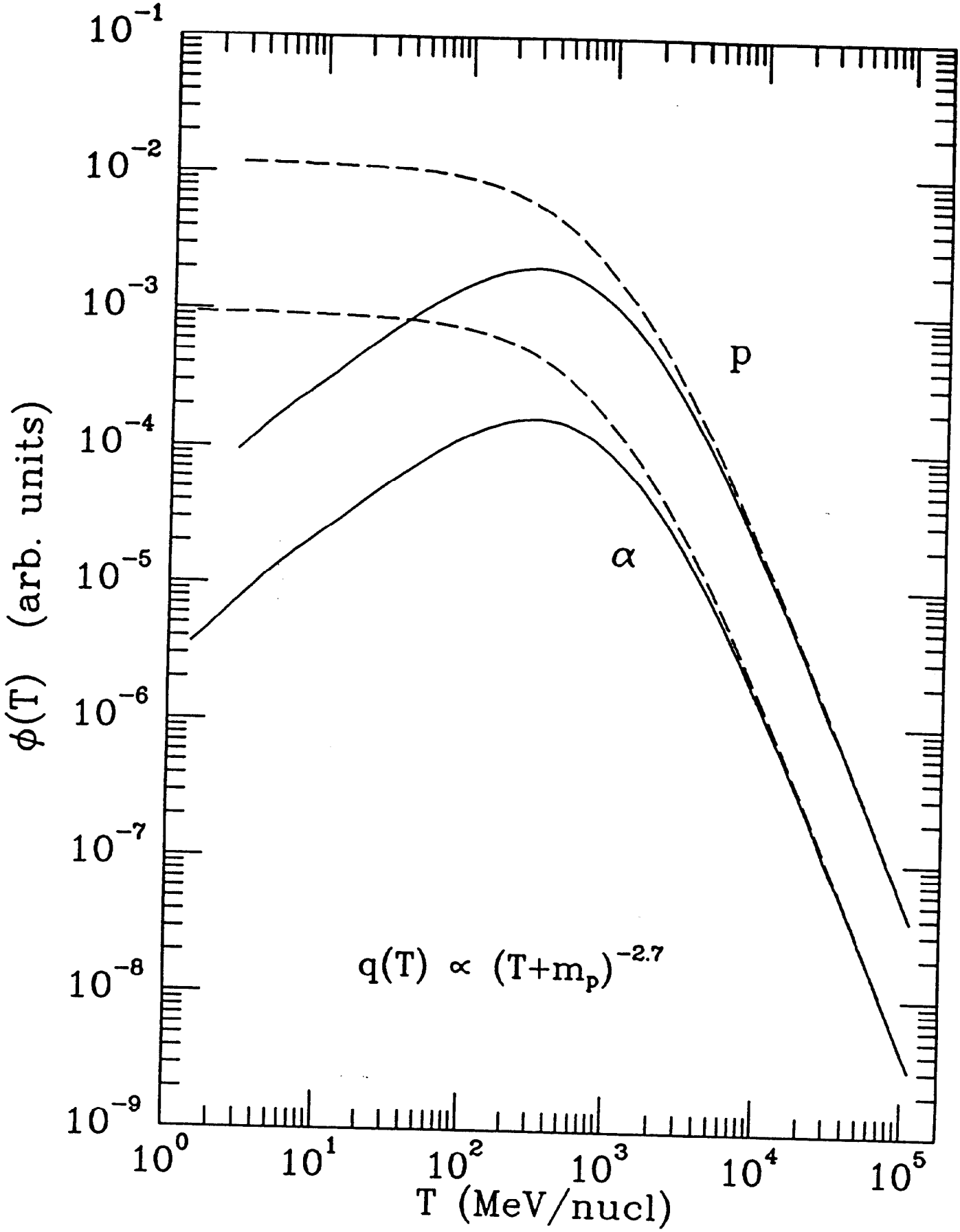
10^{-1}
10^{-2}
10^{-3}
10^{-4}
10^{-5}
10^{-6}
10^{-7}
10^{-8}
10^{-9}
$\phi(T)$ (arb. units)
p
α
$q(T) \propto (T+m_p)^{-2.7}$
10^0
10^1
10^2
10^3
10^4
10^5
T (MeV/nucl)

FIG 1(b)

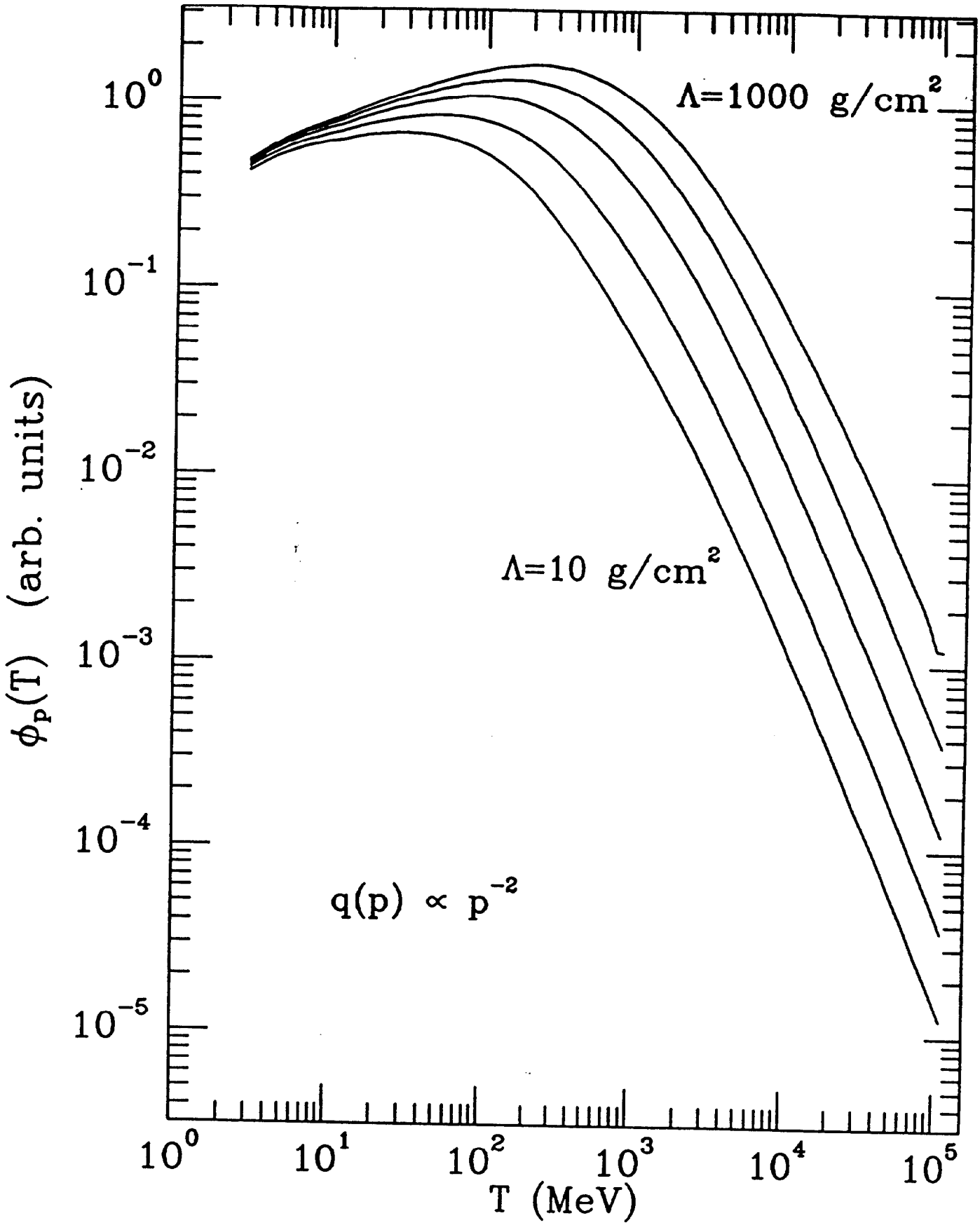
Λ=1000 g/cm²
Λ=10 g/cm²
q(p) ∝ p⁻²
φp(T) (arb. units)
T (MeV)
10⁰
10⁻¹
10⁻²
10⁻³
10⁻⁴
10⁻⁵
10⁰
10¹
10²
10³
10⁴
10⁵

FIG 2(a)

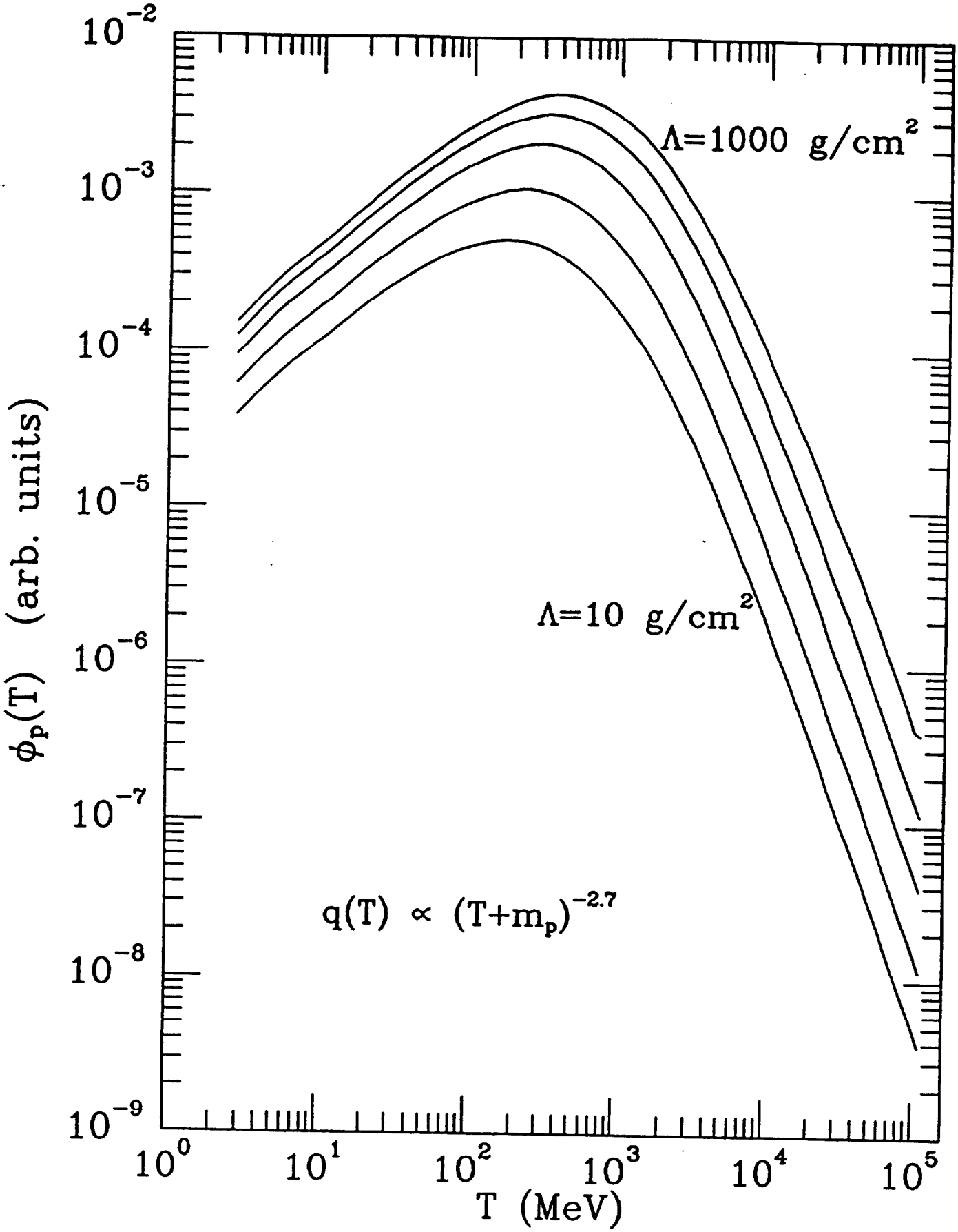
10^{-2}
10^{-3}
10^{-4}
10^{-5}
10^{-6}
10^{-7}
10^{-8}
10^{-9}
$\phi_p(T)$ (arb. units)
Λ=1000 g/cm^2
Λ=10 g/cm^2
$q(T) \propto (T+m_p)^{-2.7}$
10^0
10^1
10^2
10^3
10^4
10^5
T (MeV)

FIG 2 (b)

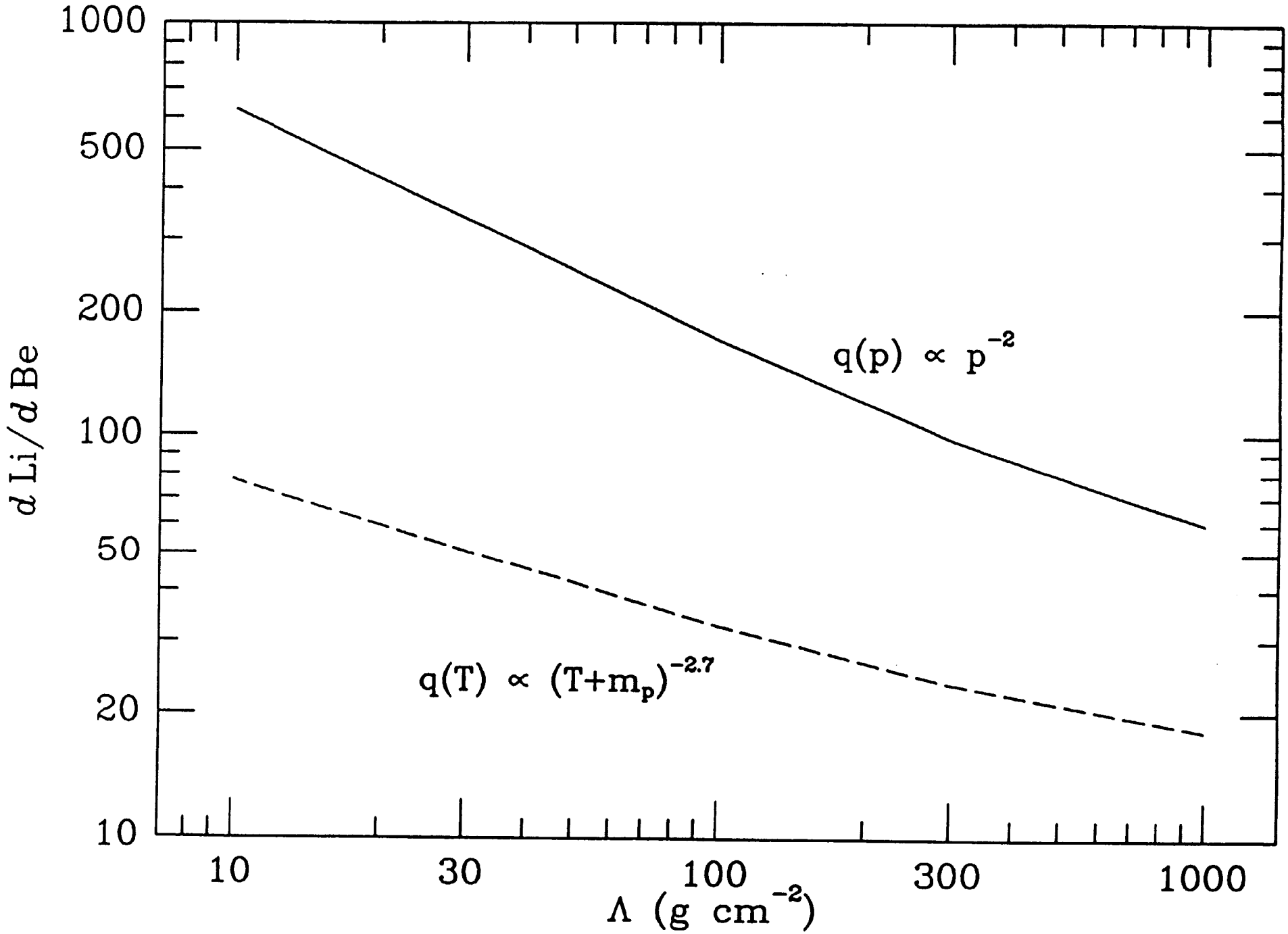
1000
500
200
100
50
20
10
d Li/d Be
q(p) ∝ p^-2
q(T) ∝ (T+m_p)^-2.7
10
30
100
300
1000
Λ (g cm^-2)

FIG 3

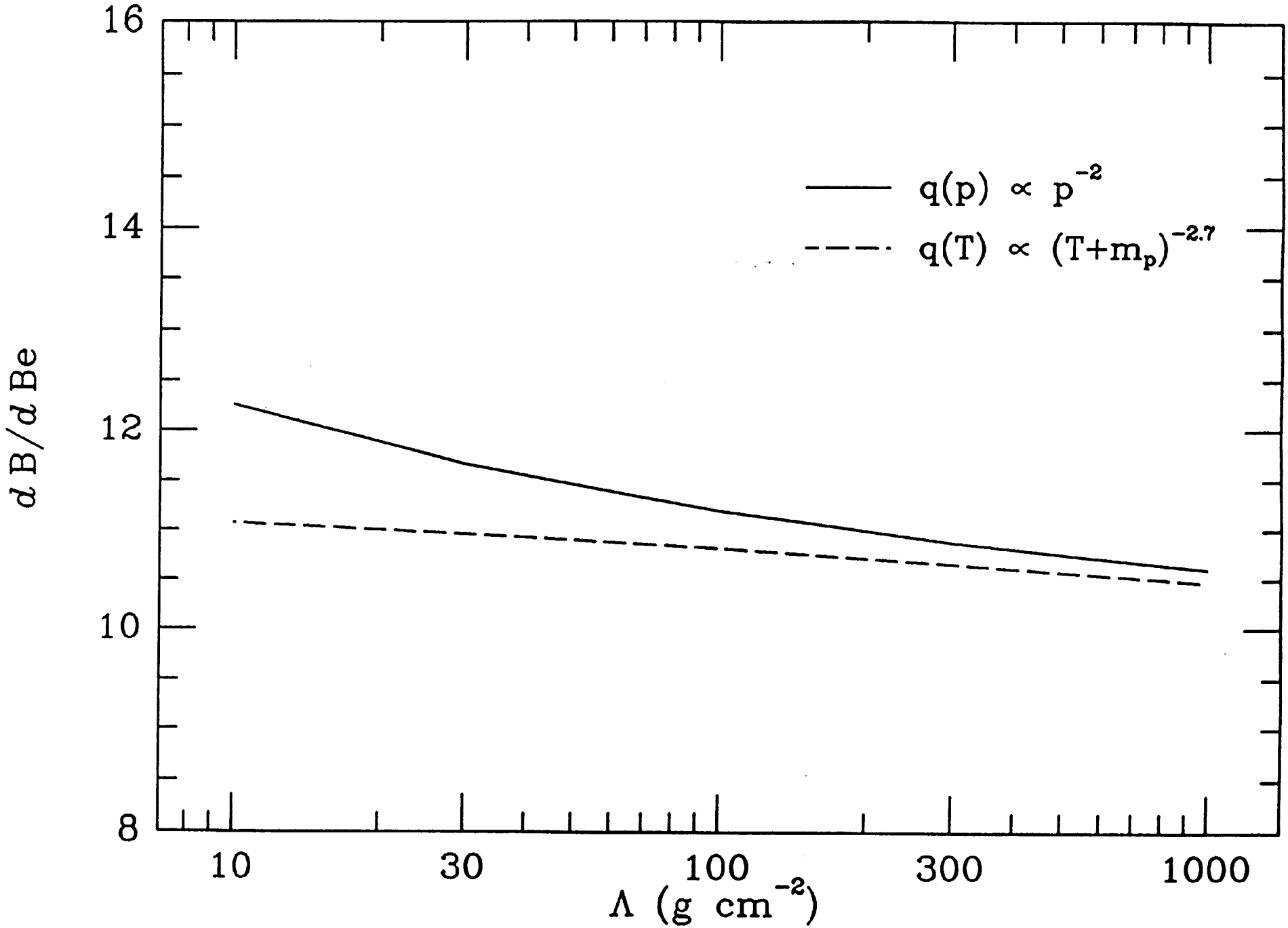

FIG 4

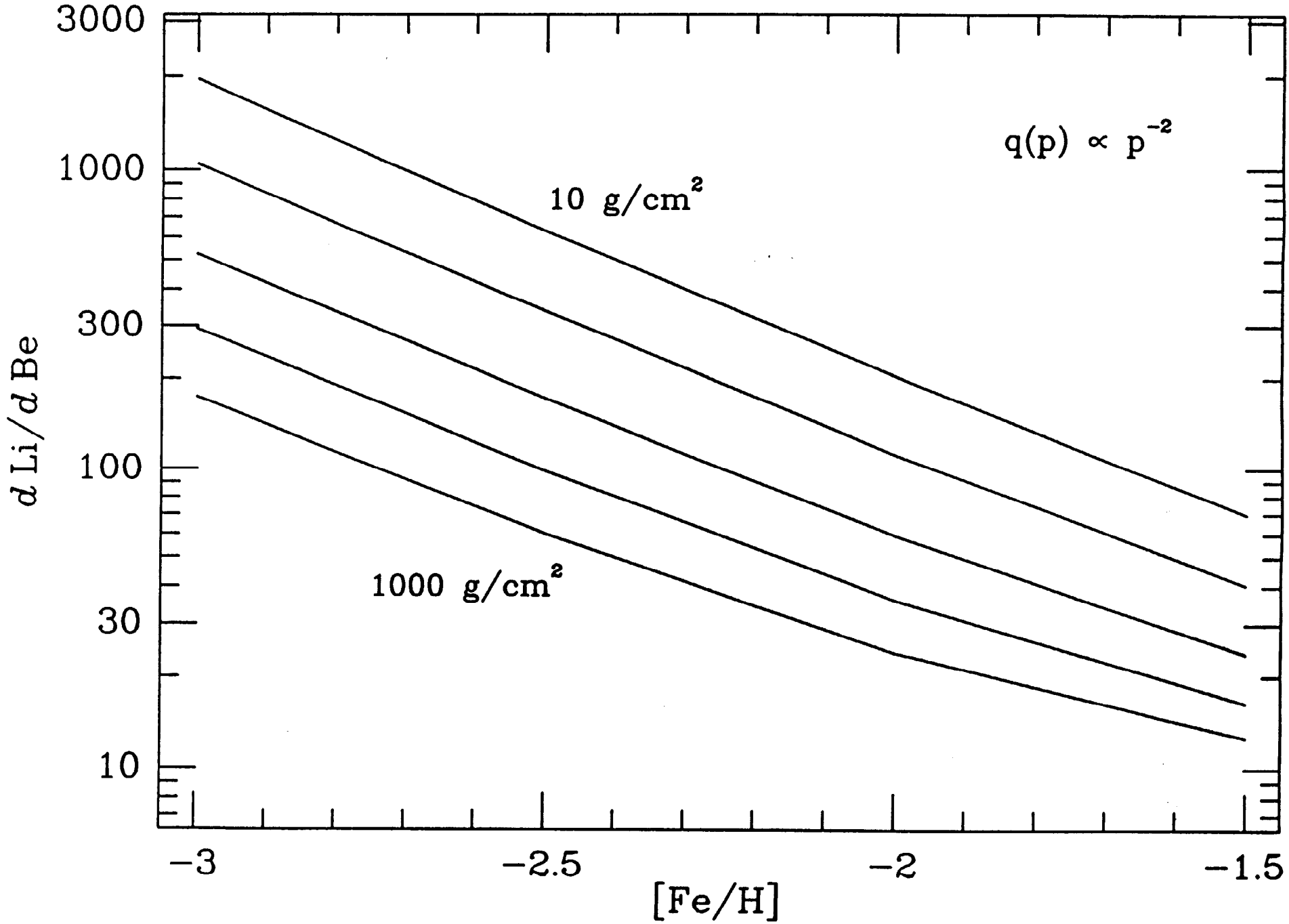
3000
1000
300
100
30
10
d Li/d Be
q(p) ∝ p^-2
10 g/cm^2
1000 g/cm^2
−3
−2.5
−2
−1.5
[Fe/H]

FIG 5 (a)

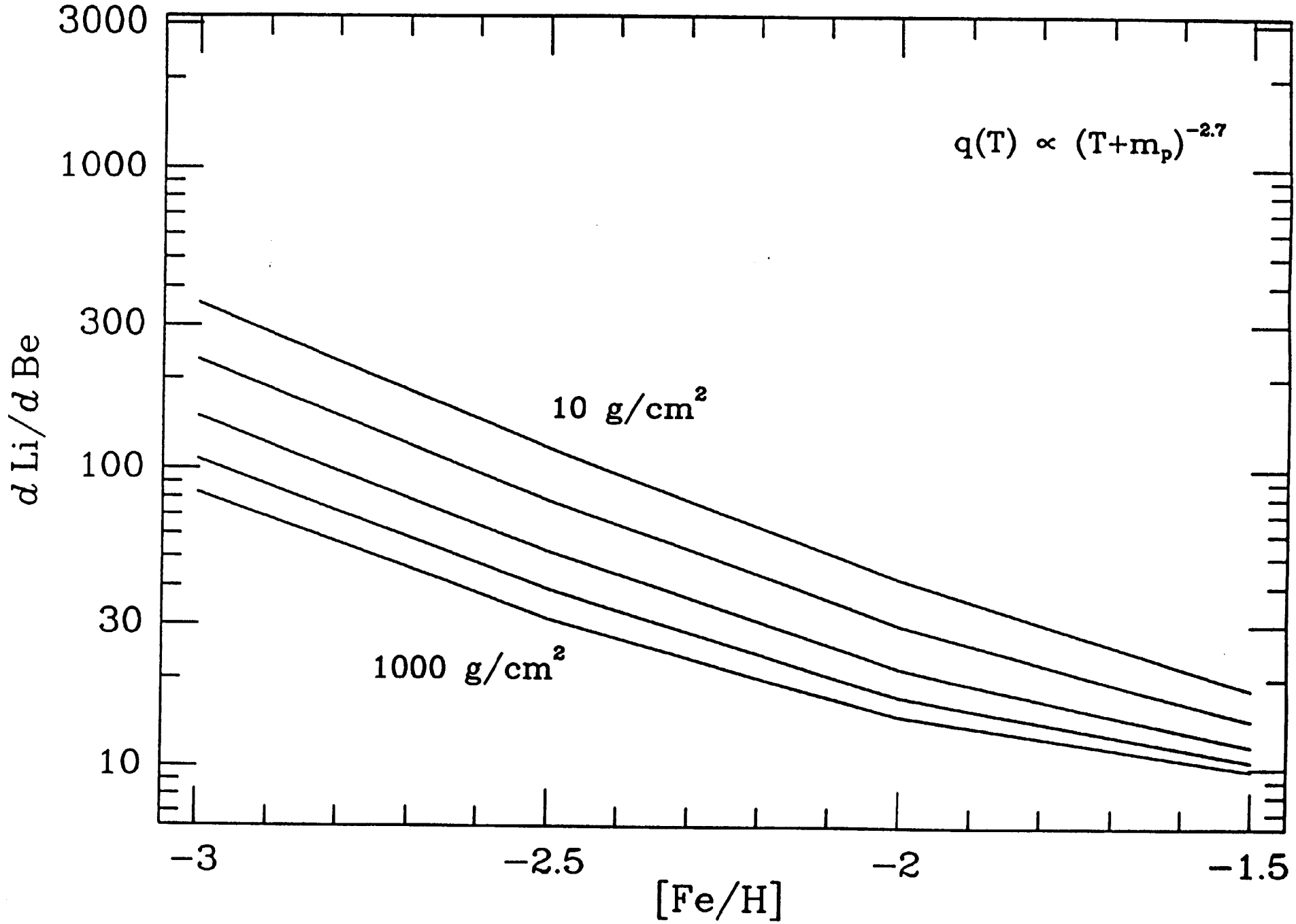
3000
1000
300
100
30
10
d Li/d Be
q(T) ∝ (T+m_p)^-2.7
10 g/cm²
1000 g/cm²
−3
−2.5
−2
−1.5
[Fe/H]

FIG 5 (b)

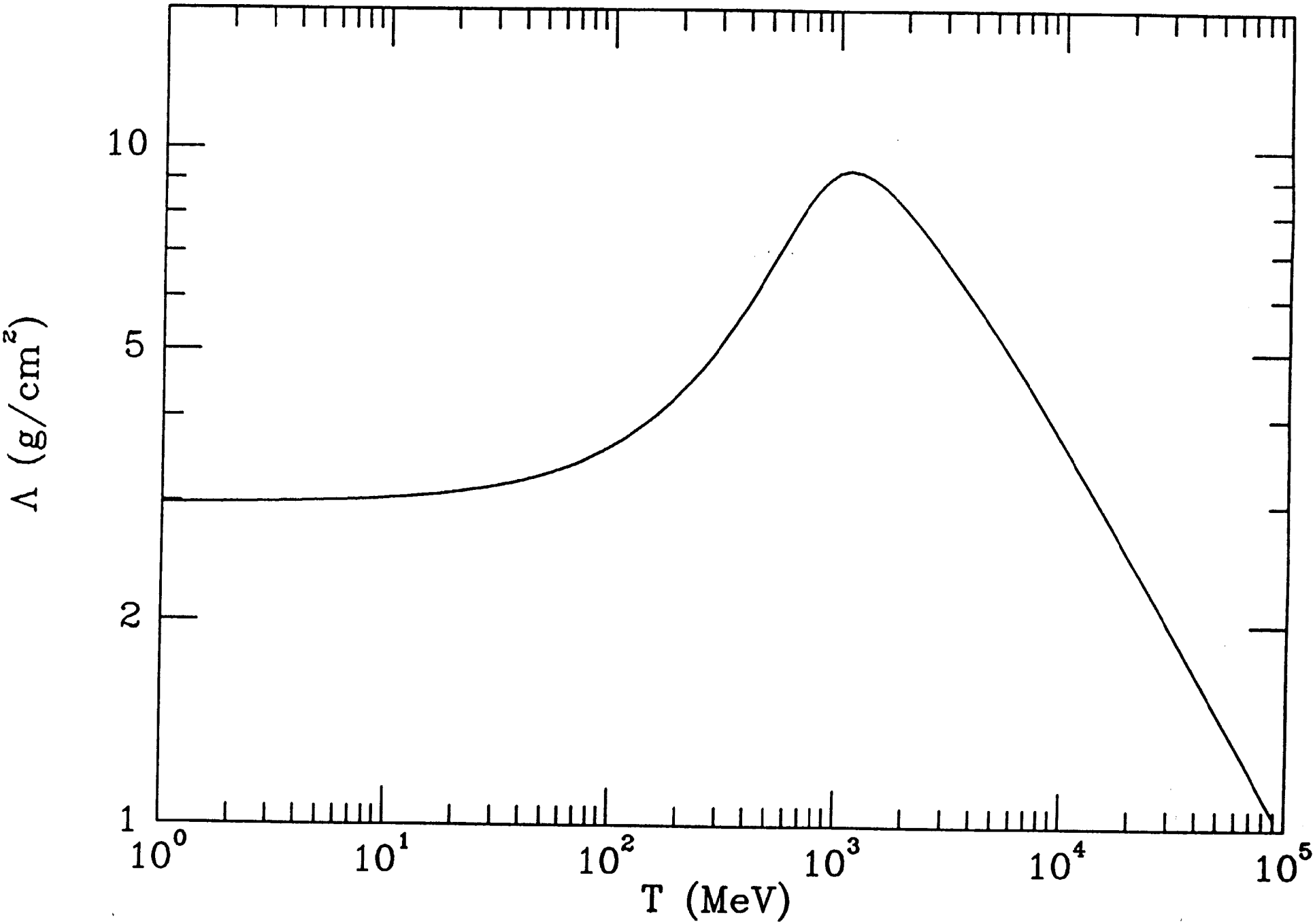

FIG 6

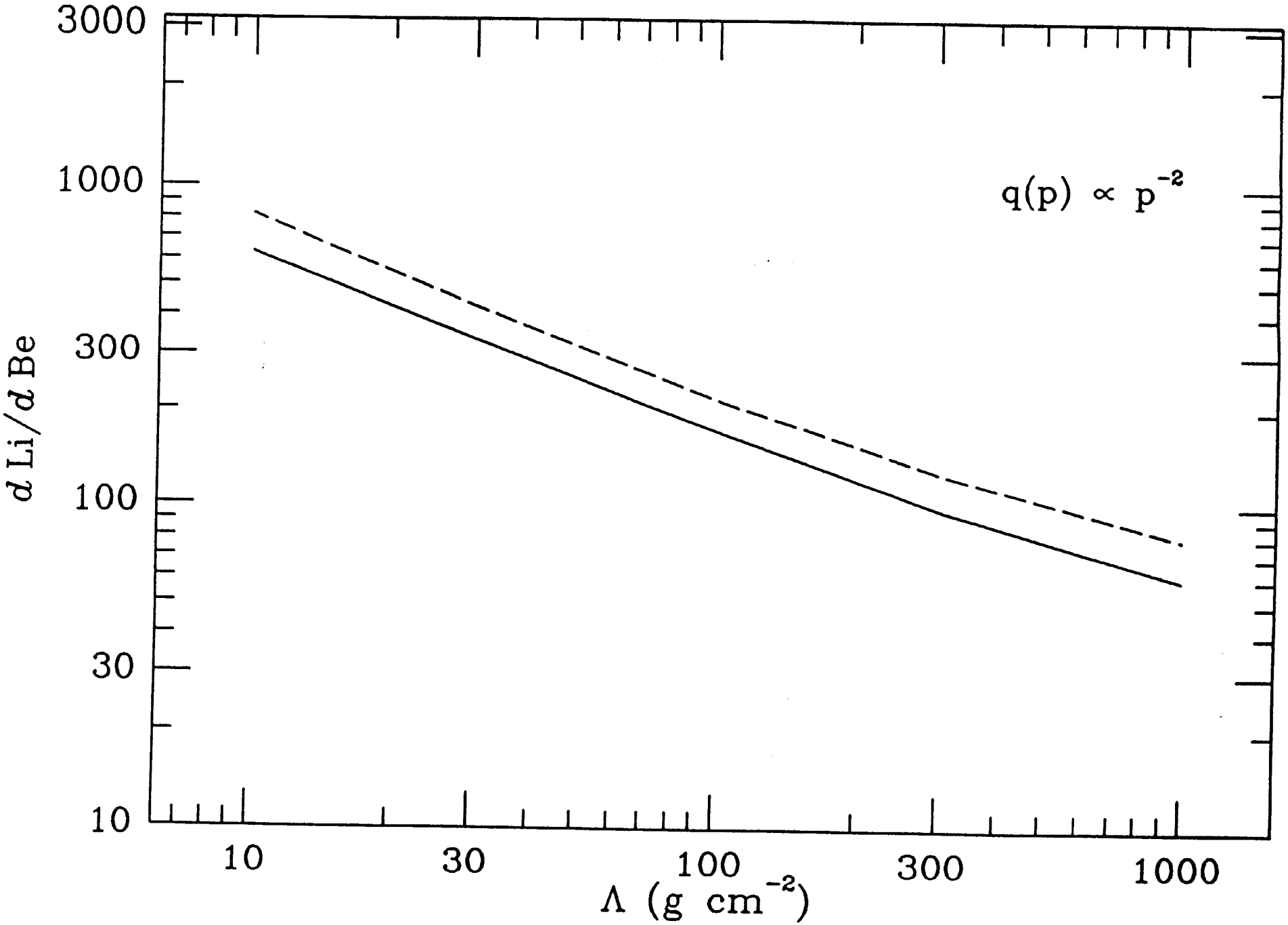

FIG 7(a)

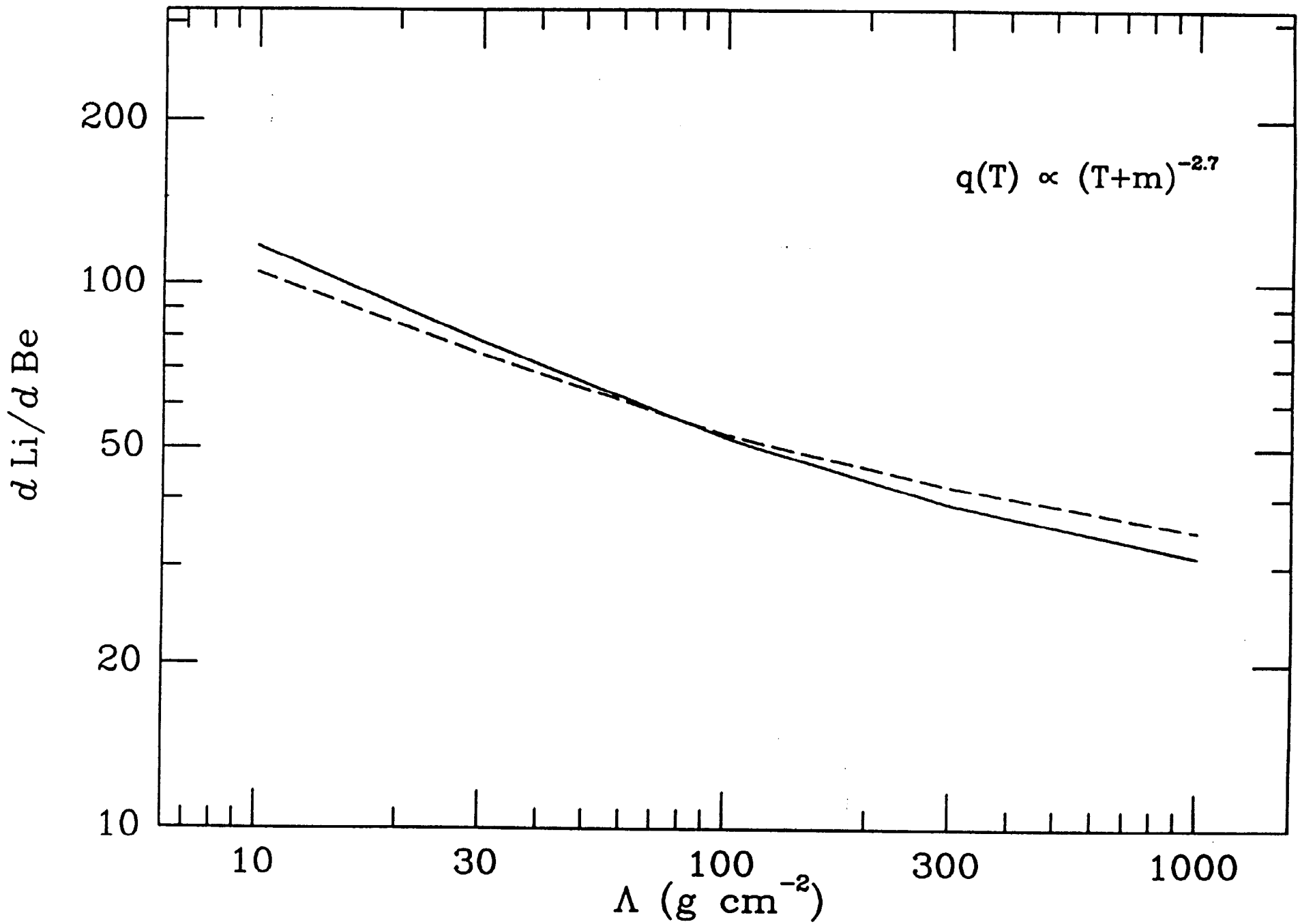

FIG 7(b)

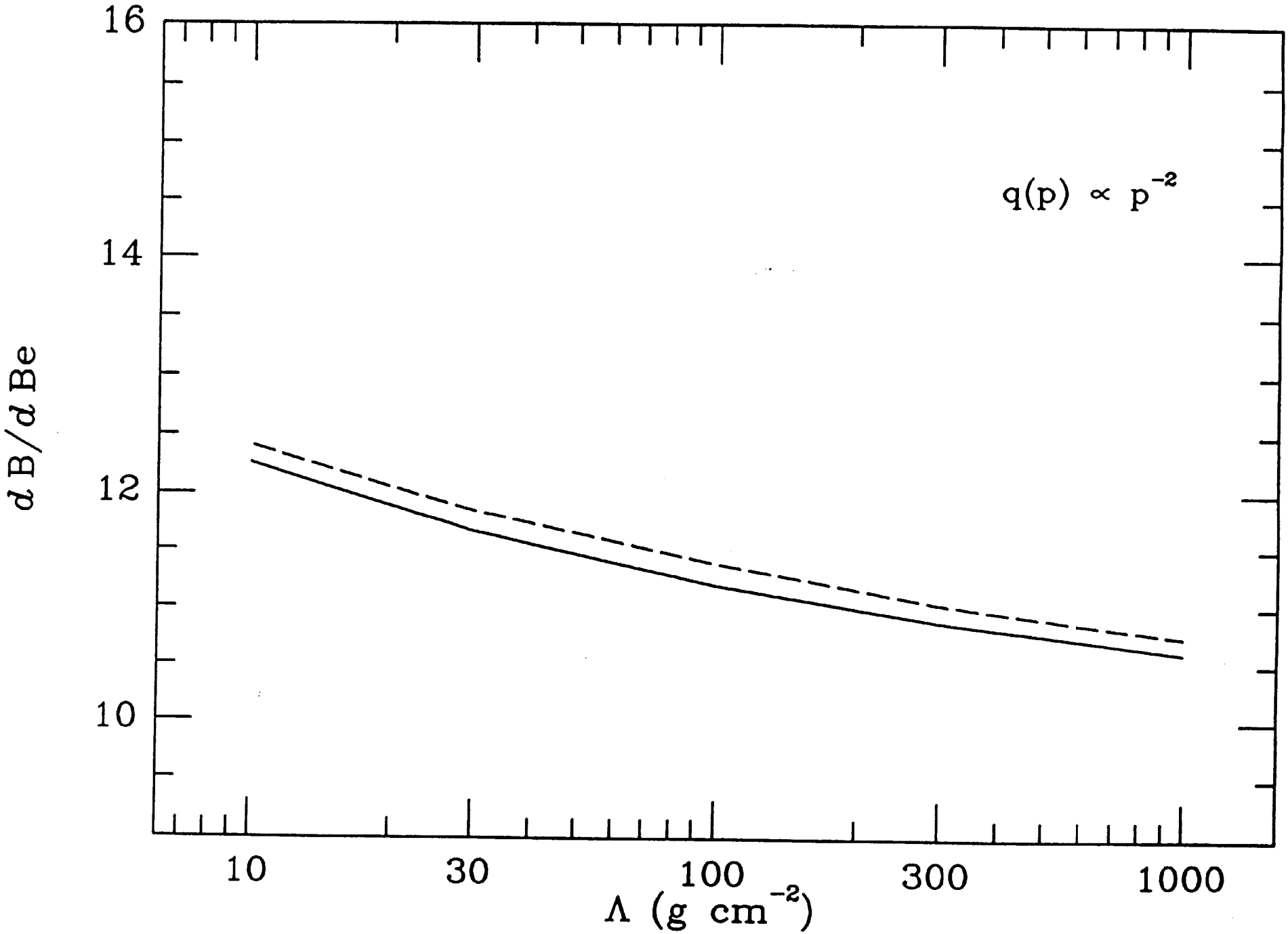

FIG 8 (a)

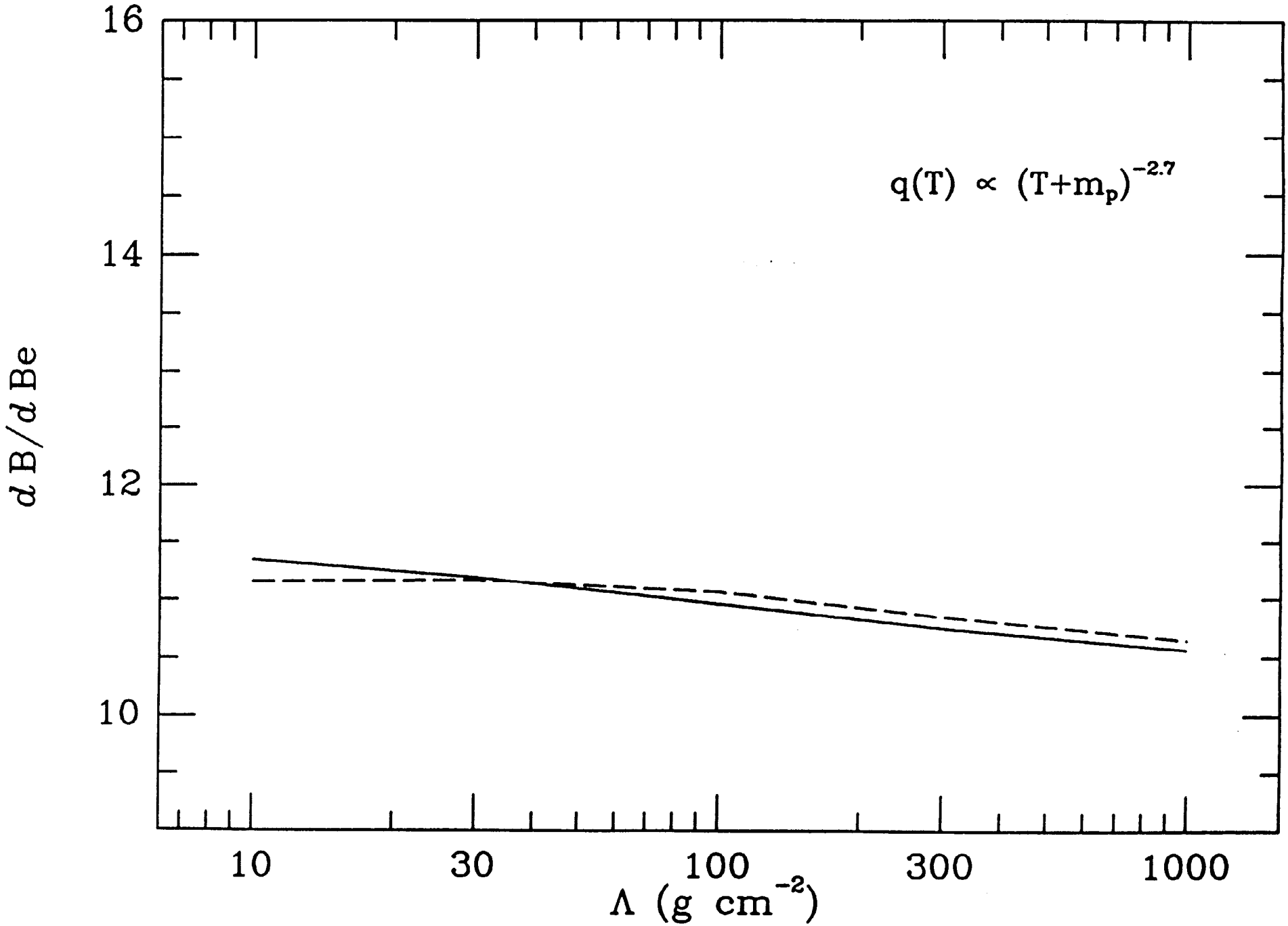

FIG 8 (b)

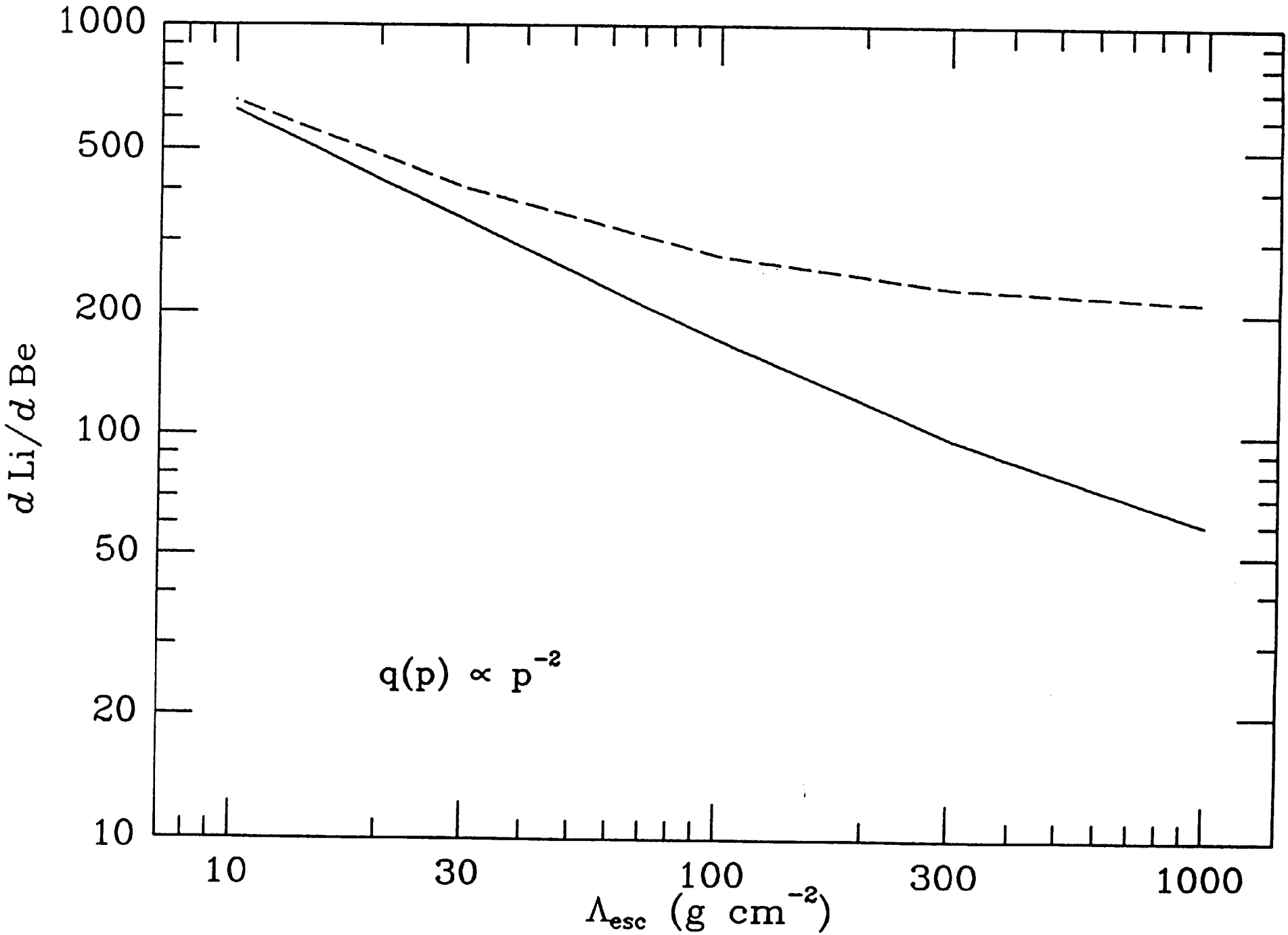
1000
500
200
100
50
20
10
d Li/d Be
q(p) ∝ p^-2
10
30
100
300
1000
Λesc (g cm^-2)

FIG 9(a)

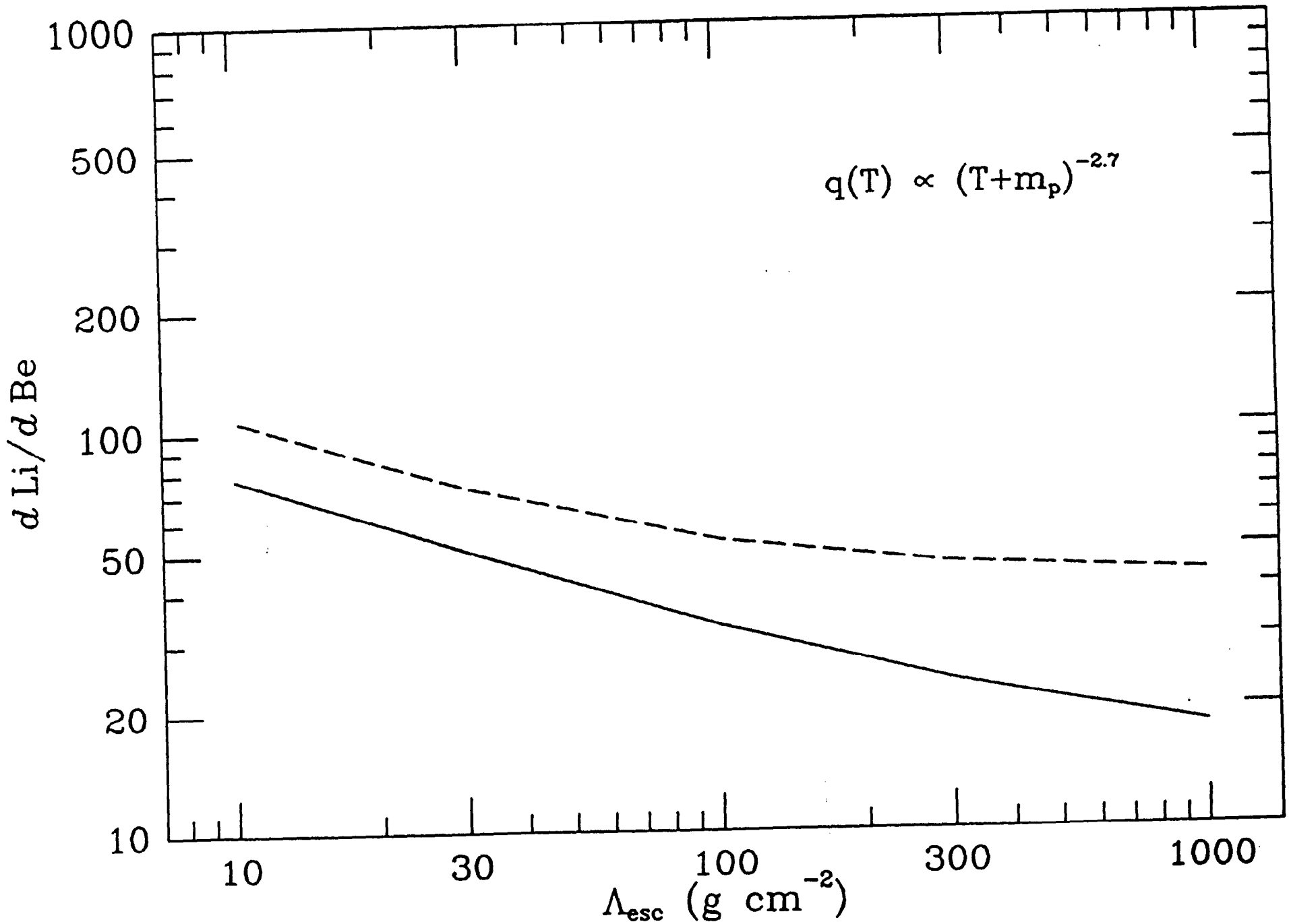
1000
500
200
100
50
20
10
d Li/d Be
q(T) ∝ (T+m_p)^-2.7
10
30
100
300
1000
Λ_esc (g cm^-2)

FIG 9(b)

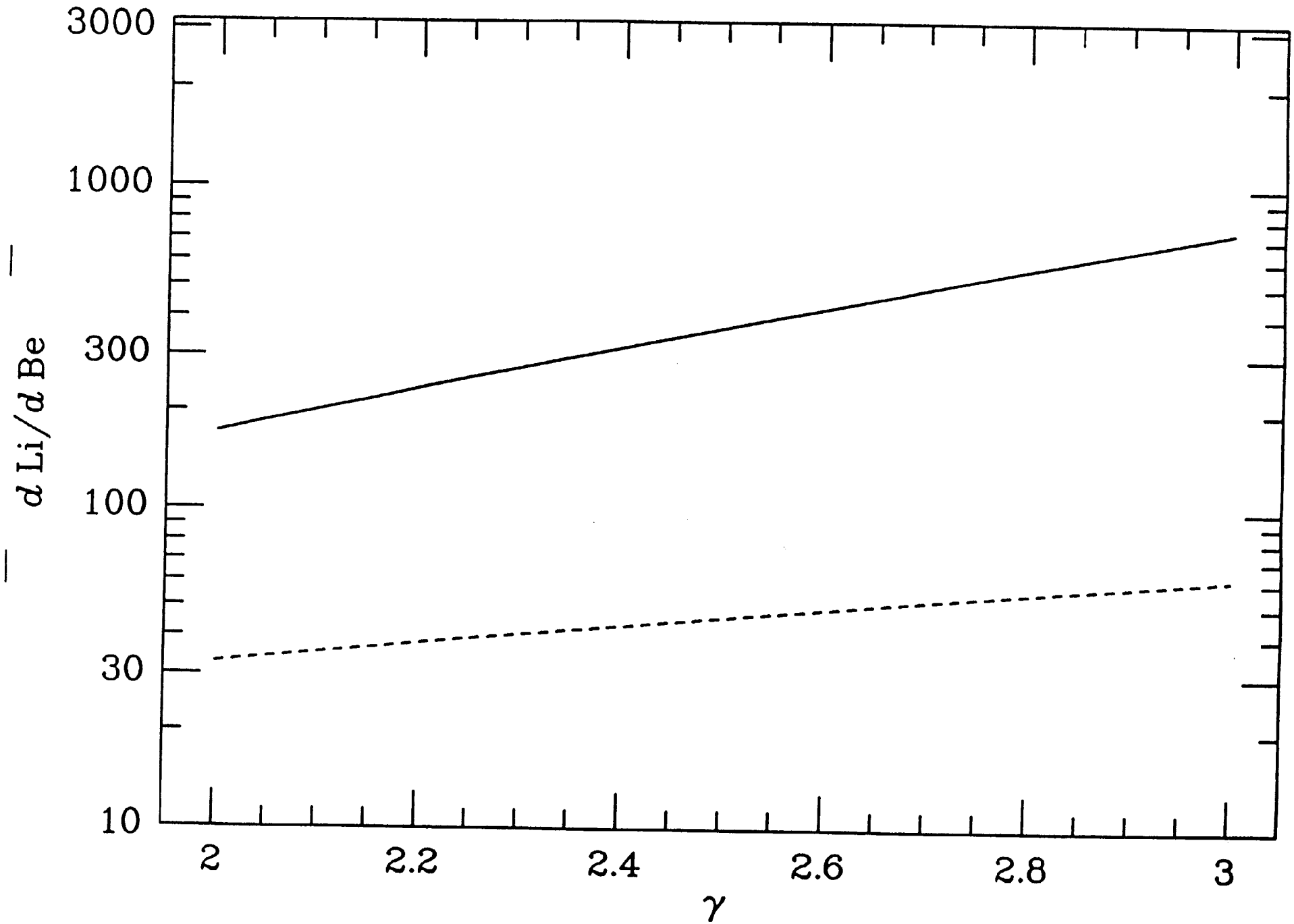

FIG 10

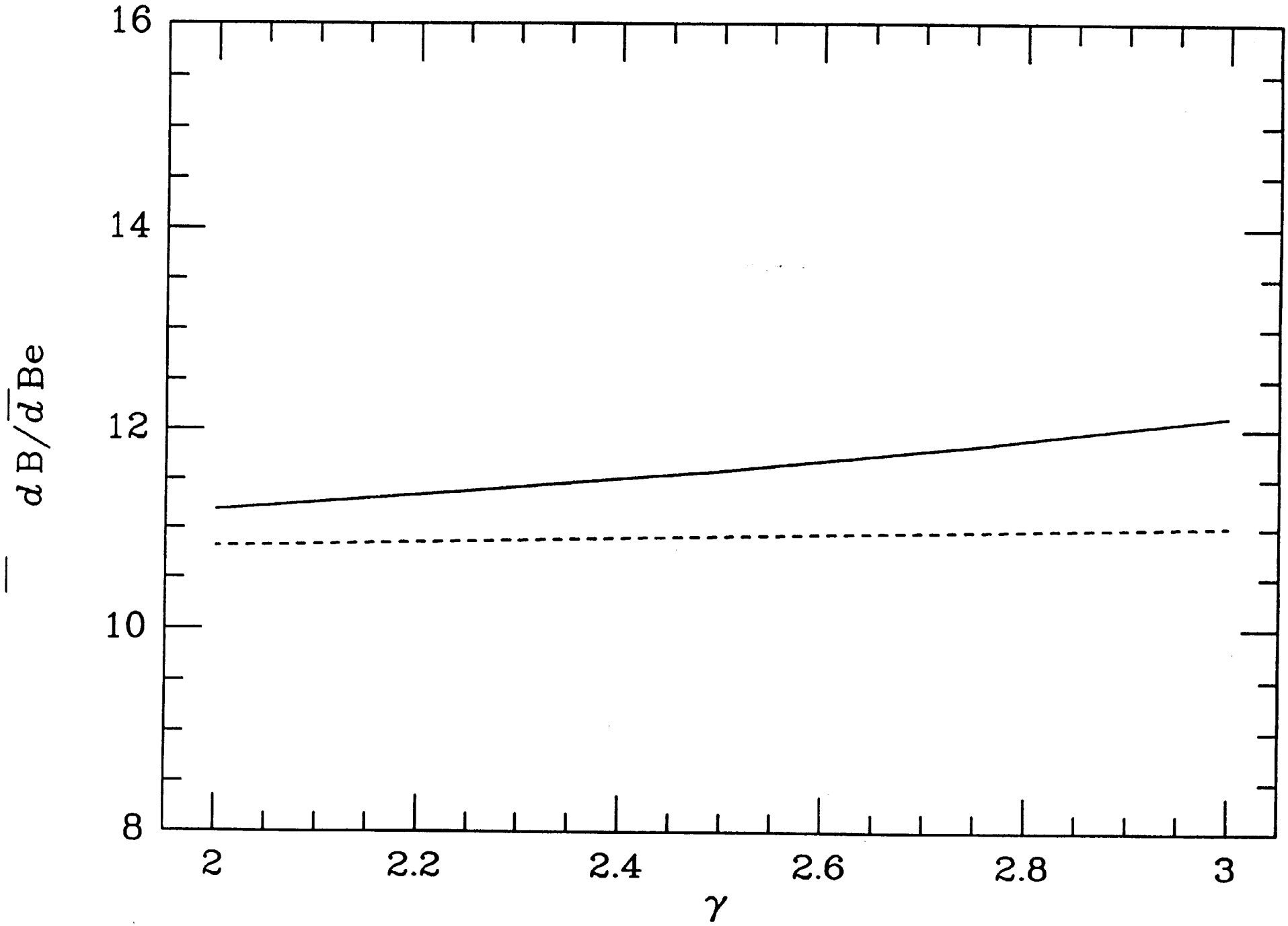

FIG 11

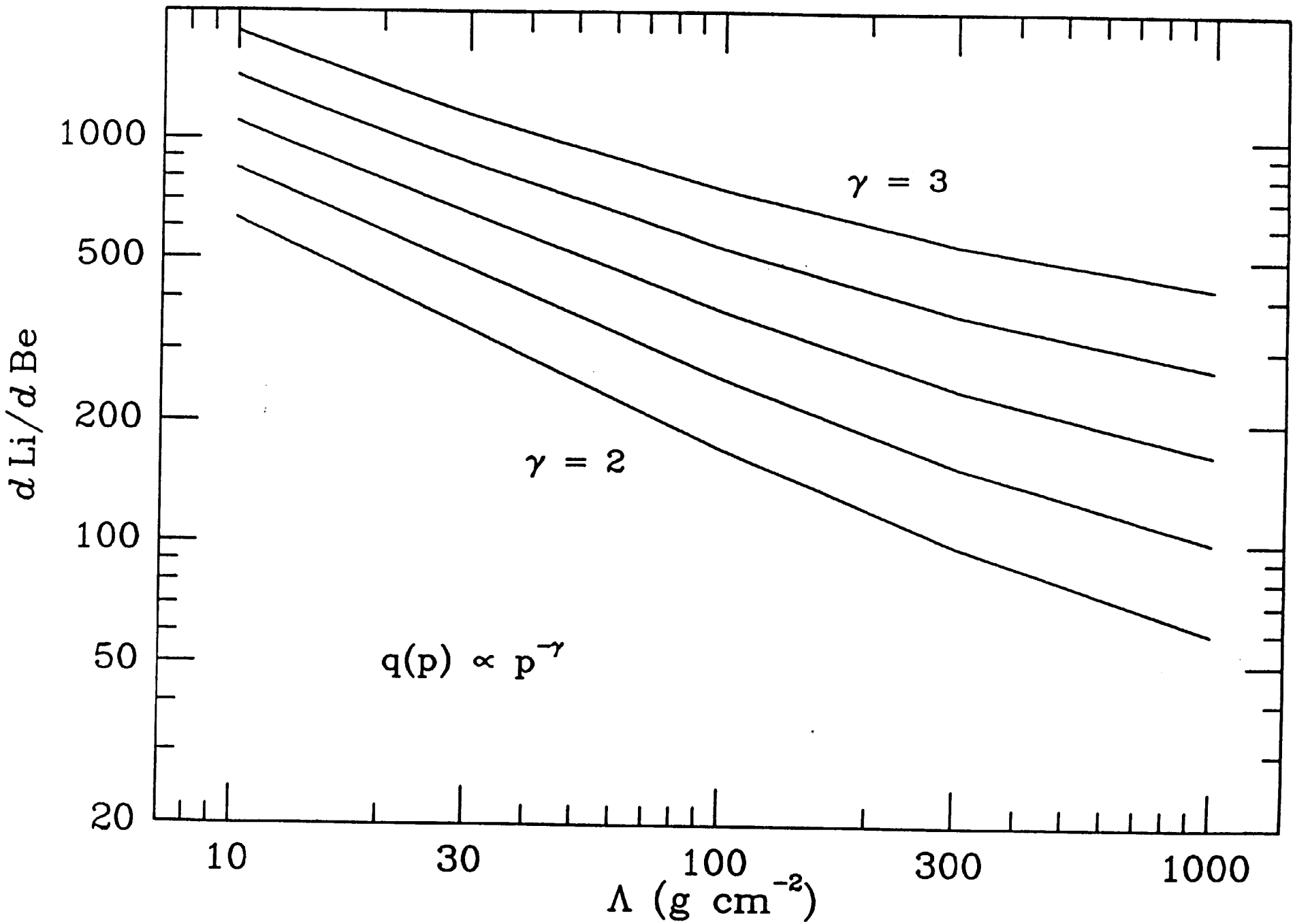
1000
500
200
100
50
20
d Li/d Be
γ = 3
γ = 2
q(p) ∝ p^−γ
10
30
100
300
1000
Λ (g cm^−2)

FIG 12 (a)

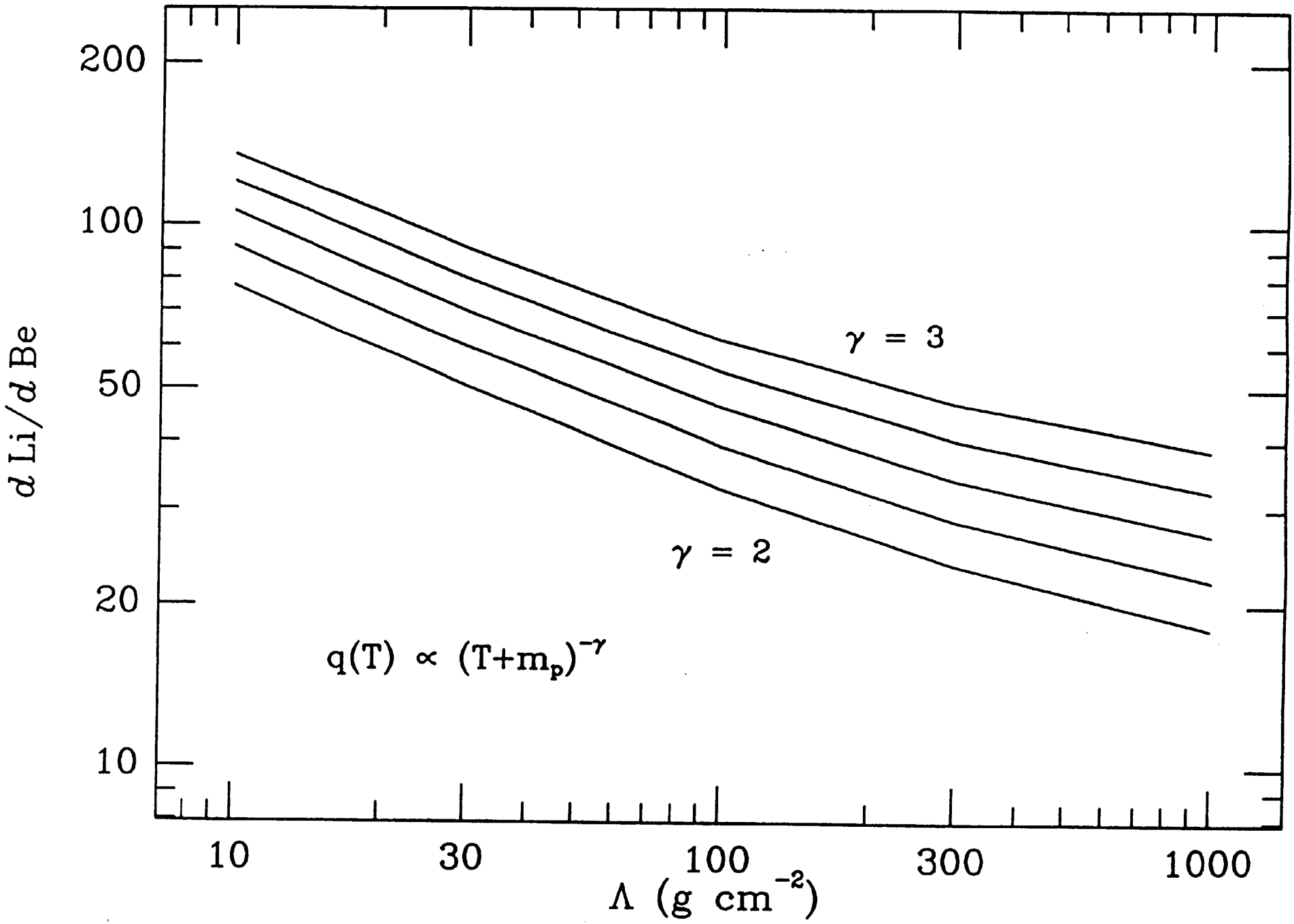

FIG 12 (b)

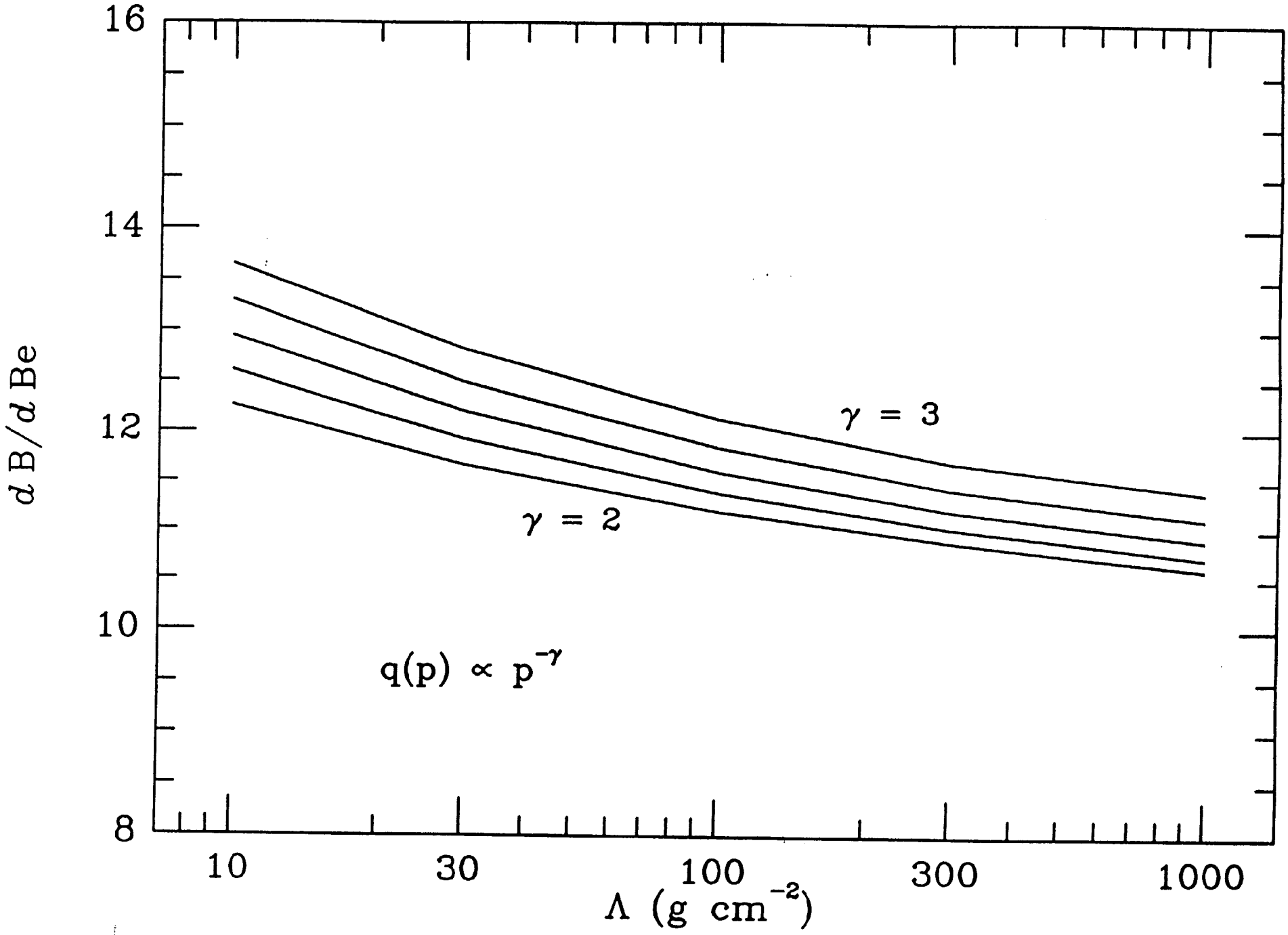

FIG 13 (a)

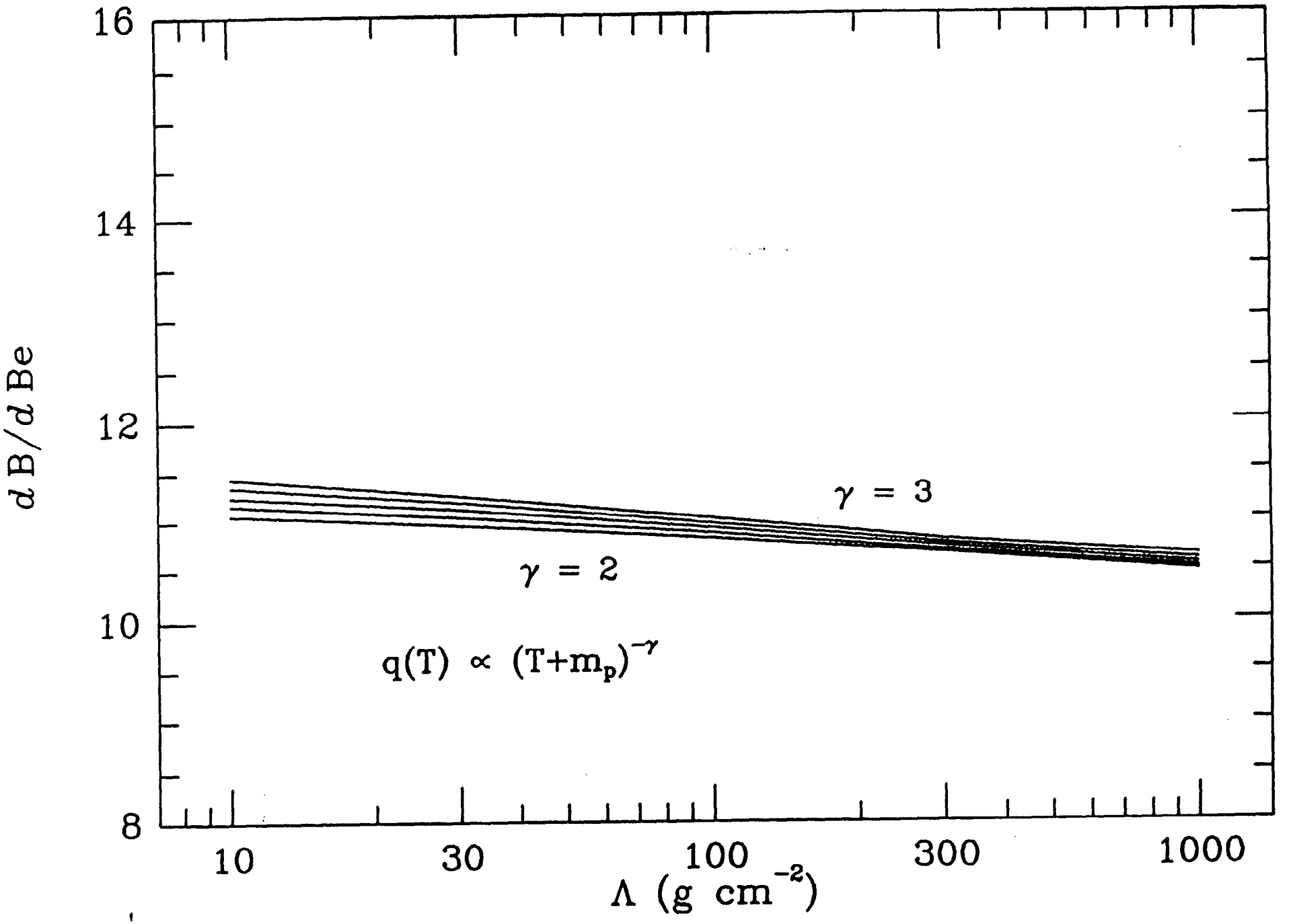

FIG 13 (b)

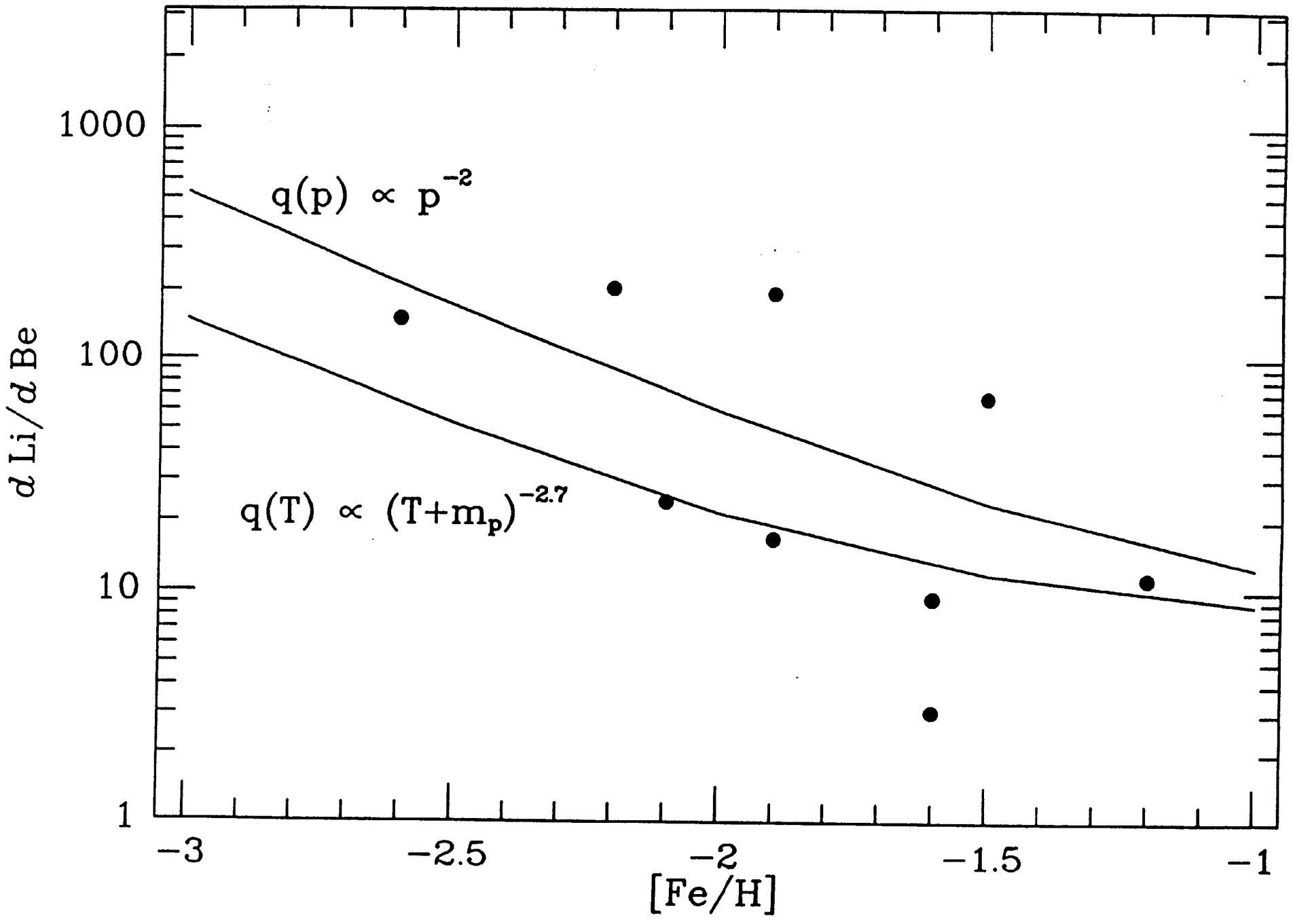

FIG 14

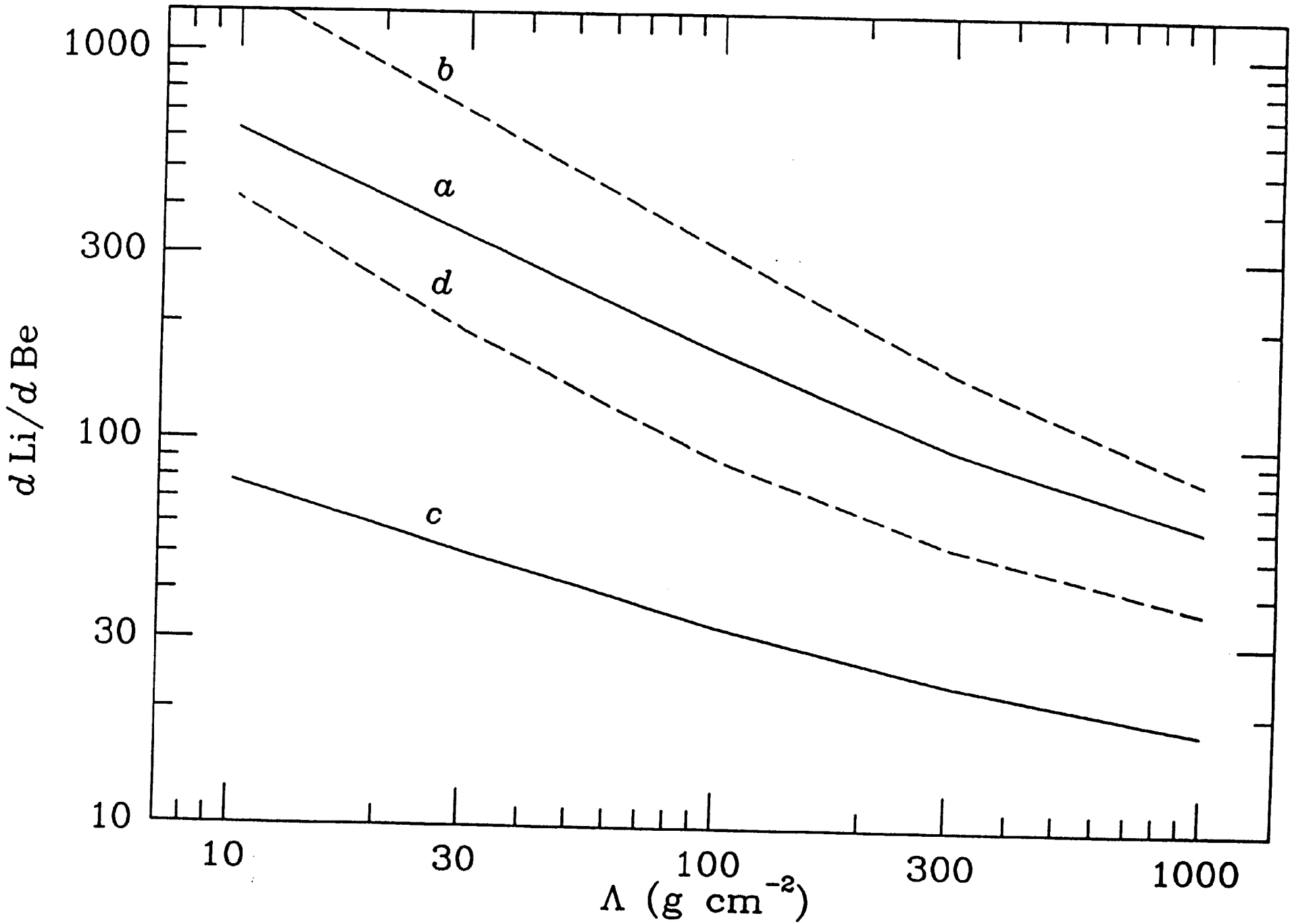

FIG 15

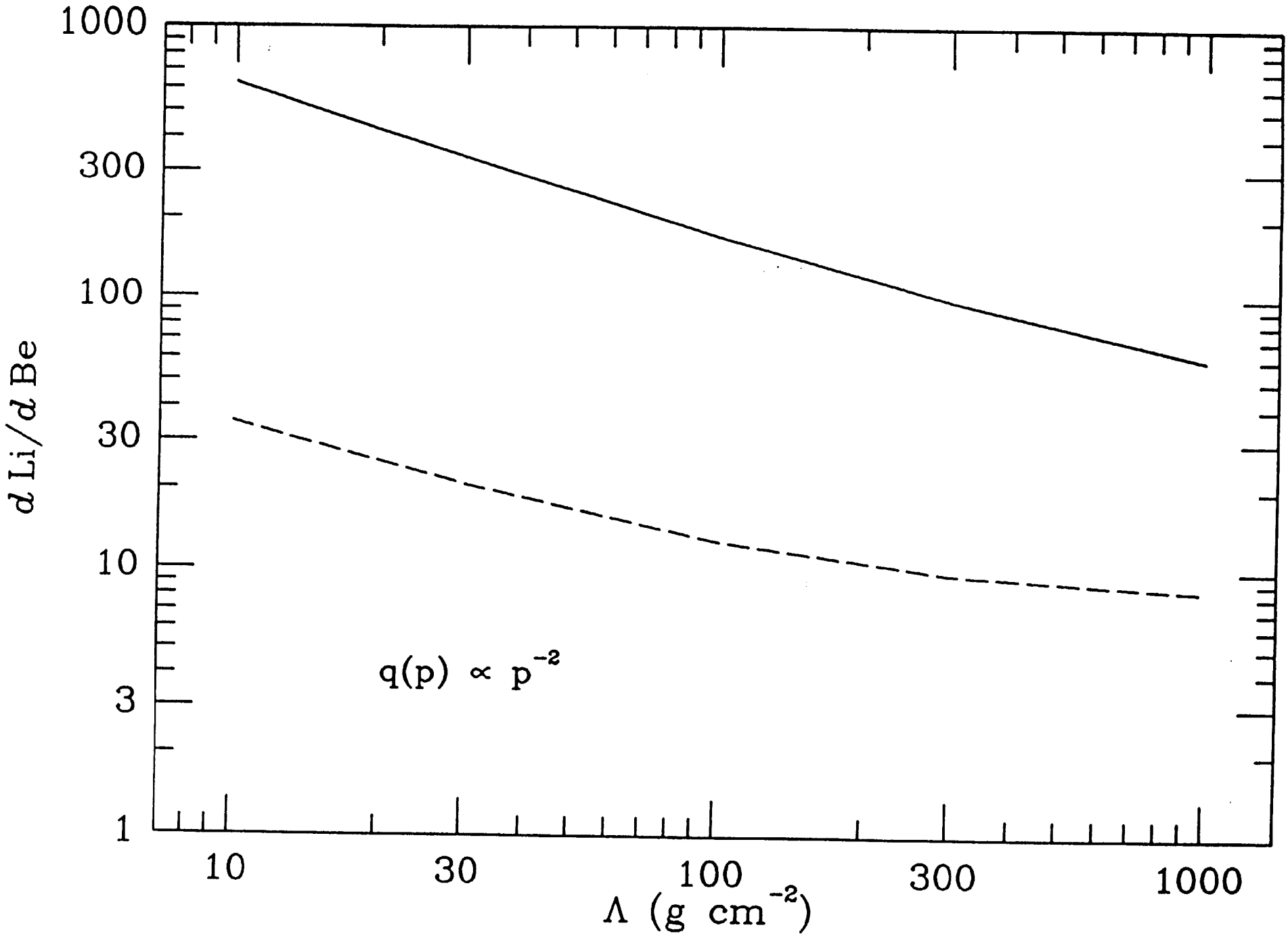

FIG 16 (a)

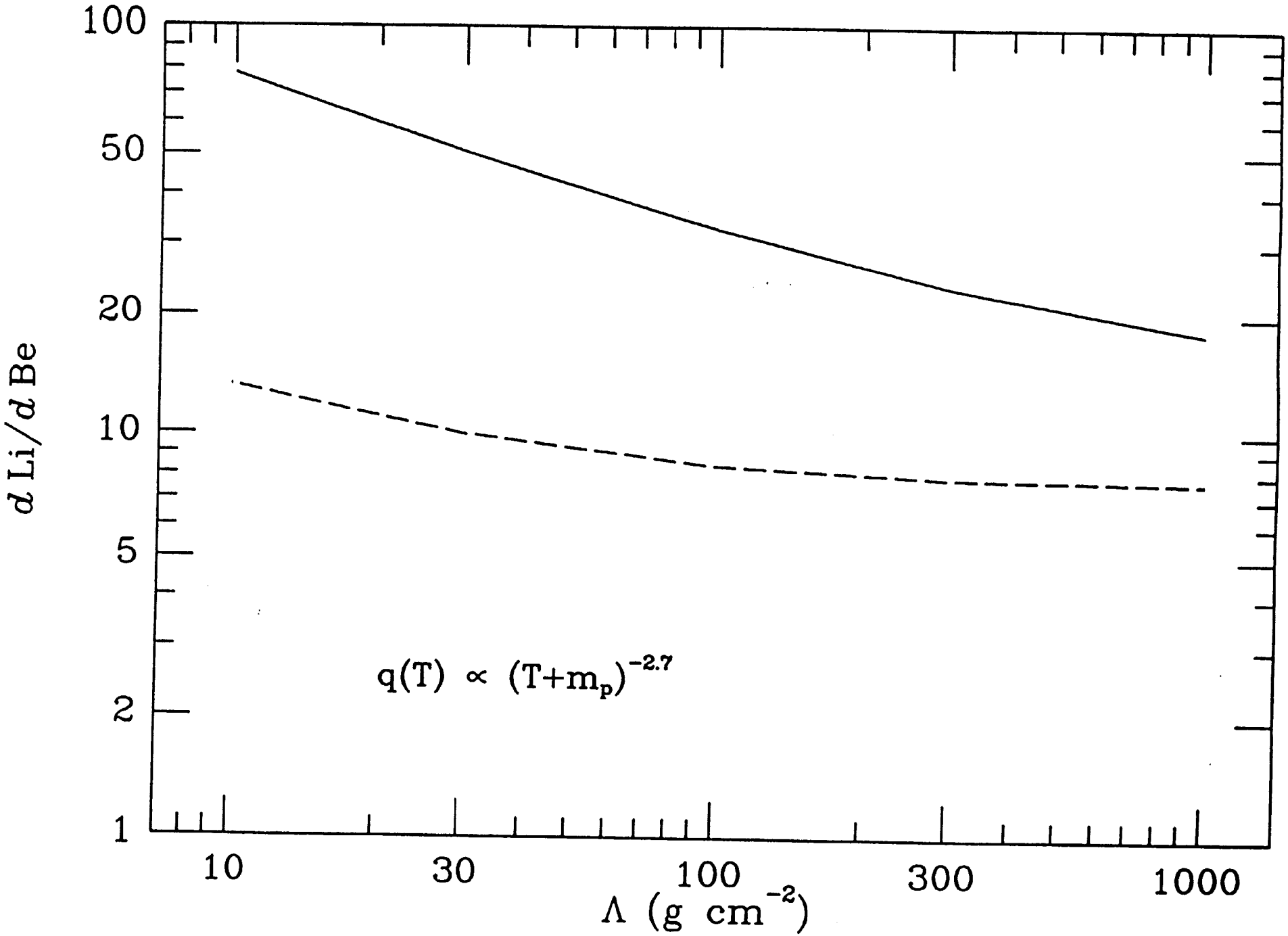

FIG 16(b)

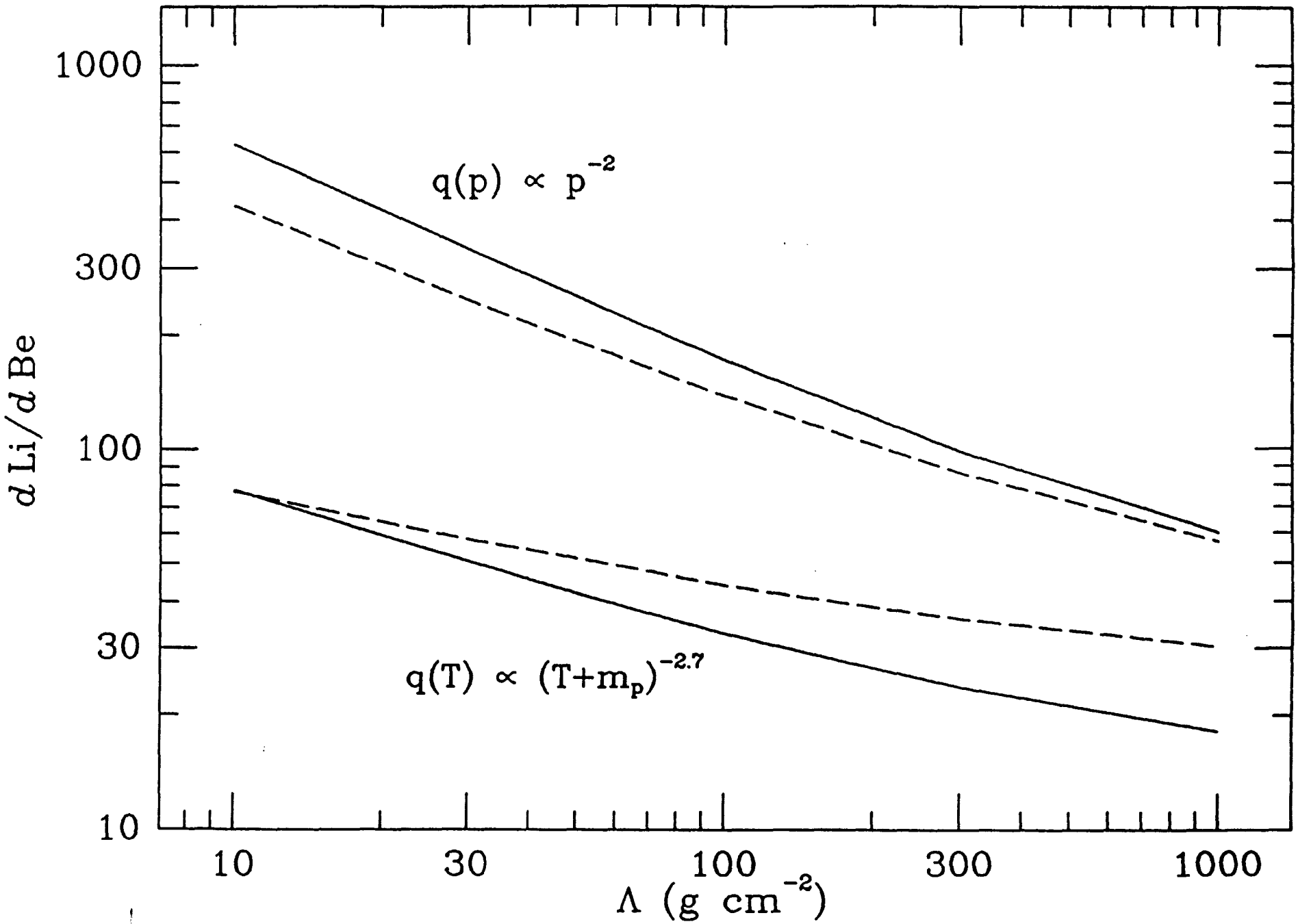
1000
300
100
30
10
d Li/d Be
q(p) ∝ p^-2
q(T) ∝ (T+m_p)^-2.7
10
30
100
300
1000
Λ (g cm^-2)

FIG 17

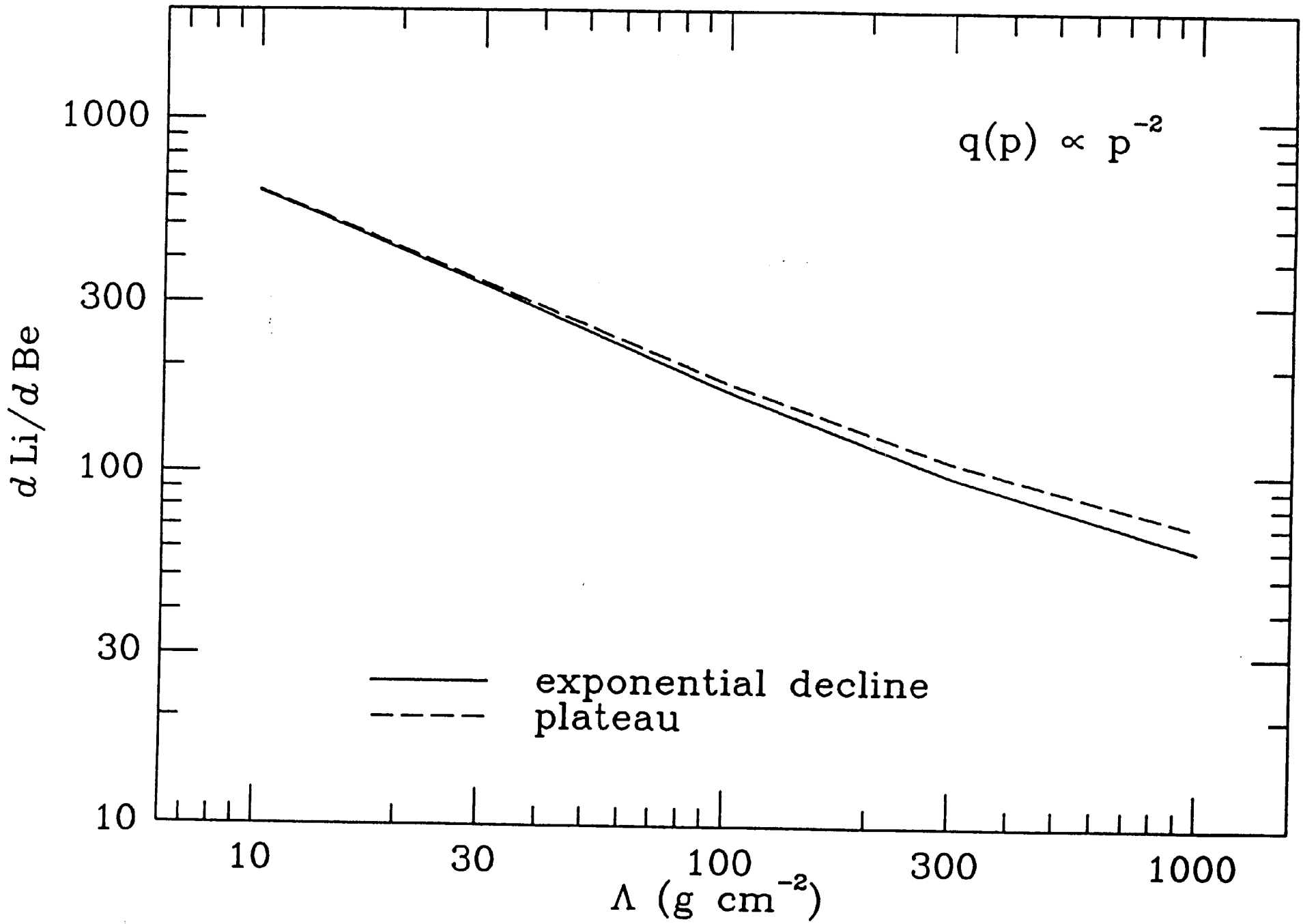
1000
300
100
30
10
d Li/d Be
q(p) ∝ p^-2
exponential decline
plateau
10
30
100
300
1000
Λ (g cm^-2)

FIG 18 (a)

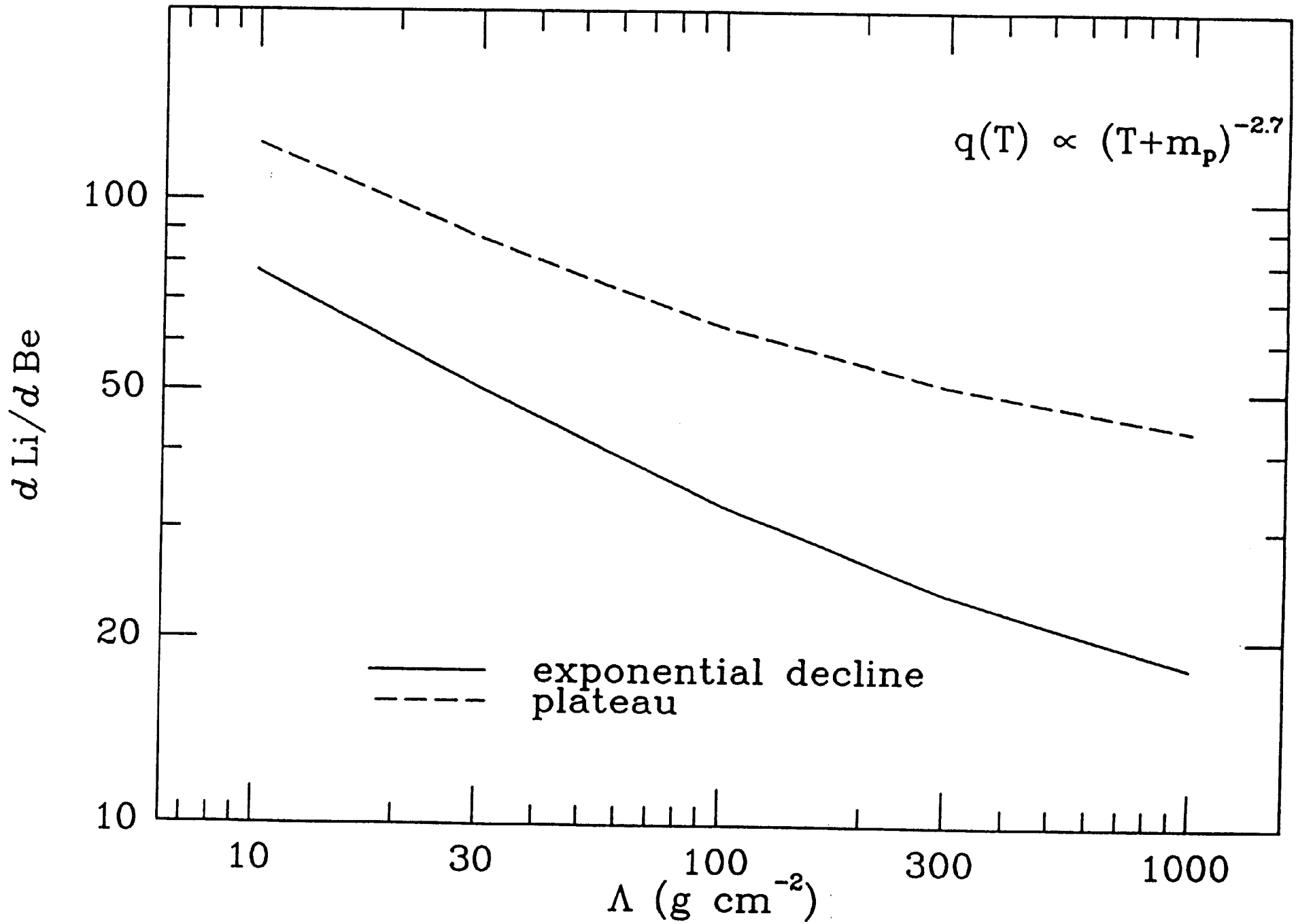
$q(T) \propto (T+m_p)^{-2.7}$
100
50
20
10
d Li/d Be
exponential decline
plateau
10
30
100
300
1000
Λ (g cm^{-2})

FIG 1B (b)